# INTRODUCTION

## EARLY HISTORY OF BETA DECAY

The discovery of radioactivity by Becquerel [BE96] at the turn and of the last century opened a new field of physics. This new property of atoms led to a search to identify the new particles emitted by certain elements and an attempt to better understand atomic structure. One of the decay processes, beta-decay, could not be explained by gravitational, electromagnetic, or strong interactions [SC66]. A new fundamental interaction (known today as the weak interaction) had to be developed [FE33] to explain this decay, thus making it very important for the investigation of nuclear structure and it was the first evidence of nuclear instability in certain energy states [RO55]. Today beta-decay is found to be very wide spread and is an important tool for nuclear structure study.

Rutherford was the first to identify (via range measurements) the new particles emitted from radioactive material known today as beta-particles or electrons [RU03]. As early as 1910 studies on beta-decays showed that the emitted beta-particles did not have well defined energies; but had a continuous energy and momentum distribution that appeared to violate the laws of conservation of energy and momentum [HA69]. Another major problem was reconciling atomic mass and atomic number with nuclear spin. The concept that nuclei consisted of protons and electrons did not always predict the correct nuclear spin. If electrons existed in the nucleus, then the spins measured for odd atomic number and even atomic mass elements did not fit theoretical predictions. One example is the deuterium nucleus with Atomic Number 1 and Atomic Mass 2. This nucleus should contain two protons and one electron giving a half integral spin; however, its ground state has spin $1^+$.

The solution to the problem of energy and momentum conservation came in 1931

when Pauli postulated that a second particle was emitted with the beta-particle that he called the neutron [PA34]. Later Fermi called this elusive particle the neutrino [FE33]. This postulate did not violate conservation of energy and momentum because the decay involved three particles allowing a continuous energy and momentum distribution for the beta-particles. Then in 1932, Chadwick [CH32] discovered the neutron and solved the spin problem associated with the spin of odd-odd nuclei. The deuterium nucleus consist of two spin 1/2 particles giving the observed integral spin.

## Formalism of Beta Decay Theory

In 1933 Fermi postulated that beta-decays could be represented by a model similar to the electromagnetic interaction process of the emission and absorption of light quanta [FE33]; however, it was much more complicated than electromagnetic interactions [RO55]. Fermi's proposed theory for beta-decay [FE33] has become the theoretical basis for weak interactions today. The basic assumptions for this theory were:

1) The existence of a neutrino with mass equal to zero, to uphold the principle of conservation of energy and momentum [FE33].
2) Beta-particles or electrons emitted by nuclei do not exist prior to the decay but are formed together with the neutrino in a fashion similar to how light is formed in a quantum jump in an atom [FE33].
3) The proton and neutron are two quantum states of a similar nucleon (Isospin symmetry) [FE33].
4) Beta and neutrino emissions are connected with a transition between the two quantum states of a nucleon [FE33].

Fermi used the method of "quantized probability amplitudes" to represent beta-interaction operators. He expressed the interaction Hamiltonian as:

$$H = QL(\Psi,\phi) + Q^{*}L(\Psi^{*},\phi^{*})$$

[FE33]

where L represents a bilinear expression of $\psi$ and $\phi$, Q and $Q^{*}$ are isospin lowering and raising operators, respectively [FE33]. Beta and neutrino wave functions $\psi$ and $\phi$, respectively, are non-commutative operators that act on the functions of the occupation number of the quantum states of the betas and neutrinos so that $\psi$ decreases betas by one, $\psi^{*}$ increases betas by one, $\phi$ decreases neutrinos by one, and $\phi^{*}$ increases neutrinos by one [FE33].

Fermi's theory of beta-decay allowed five forms for the interaction operators: scalar, pseudoscalar, vector, axial vector, and tensor [FE33]. The theory allowed all five forms of the interaction Hamiltonian because beta-decay does not have a macroscopic analog that one can use to apply the correspondence principle. The production of electrons are allowed by introducing the wave functions $\psi$ and $\psi^{*}$ in different terms of the energy interaction and in first approximation variations of $\psi$ and $\phi$ across the nucleus can be neglected [FE33]. Since particles are created or destroyed, one must treat the problem in terms of field theory. A nucleus is the source of the field, with the beta and neutrino as field particles [RO55]. When a nucleus changes its state of energy it involves the production of a $\beta^{-} + \bar{\nu}$ or $\beta^{+} + \nu$ [SC66]. These transitions also conserve lepton number. Prior to beta-decay the parent nucleus has a lepton number of 0. When a nucleus changes its state of energy through beta-decay the sum of lepton numbers for the daughter nucleus and emitted particles is 0 + (+1) + (-1) or 0 + (-1) + (+1), both resulting in a total lepton number of 0.

Experiments demonstrated that beta-decay is much slower than gamma-decay for same $\Delta J$; therefore, the beta-interaction had to be weak compared to the electromagnetic interaction [RO55]. Also, Fermi predicted that the transition probability for beta-decay was proportional to $E^5_{max}$. Shorter half-lives for beta-decay require larger energy, making the emission of nucleons more probable than a beta-particle [RO55]. Since the lifetime of beta-decay is very long compared to other types of radioactive decay, beta-decaying nuclei are sometimes considered "stable"; namely stable against strong interaction decay [RO55, SC66].

Angular momentum was shown to have an effect on beta-decay half-lives with the most favorable $\Delta J = 0$ or 1 [RO55]. Beta-decay experiments also showed that there is a wide distribution in the measured beta-decay half-lives for given changes in angular momentum. Fermi introduce the concept of comparative half-life or *ft* value to put all beta-decays on a common scale [FE33]. In his definition for comparative half-life he corrected the measured half-life for atomic number Z and decay energy $E_{max}$ [FE33, HA69]. This correction results in groups of log(*ft*) values for the various known beta-decays and leads to the idea of allowed and forbidden beta-decays, see figure 1.

Allowed beta-decays were originally defined as having log(*ft*) between 3 and 6, forbidden beta-decays having log(*ft*) values above 6 in general. As the understanding of beta-decay improved, a modification was made in the definition of allowed and forbidden beta-decays. Today allowed and forbidden beta-decays are defined by the orbital angular momentum (parity) carried away by the beta-neutrino system. Allowed decays are defined as decays where the beta-neutrino system carries away zero orbital angular momentum, $l = 0$ ($\Delta\pi = +$) for the beta-neutrino system, and forbidden decays are defined as decays where the beta-neutrino system carries away orbital angular momentum, $l \neq 0$. Beta-neutrino systems carrying away one unit of orbital angular momentum, $l = 1$ ($\Delta\pi = -$) for the beta-neutrino system, are defined as first-forbidden beta-decays, $l = 2$ are second-

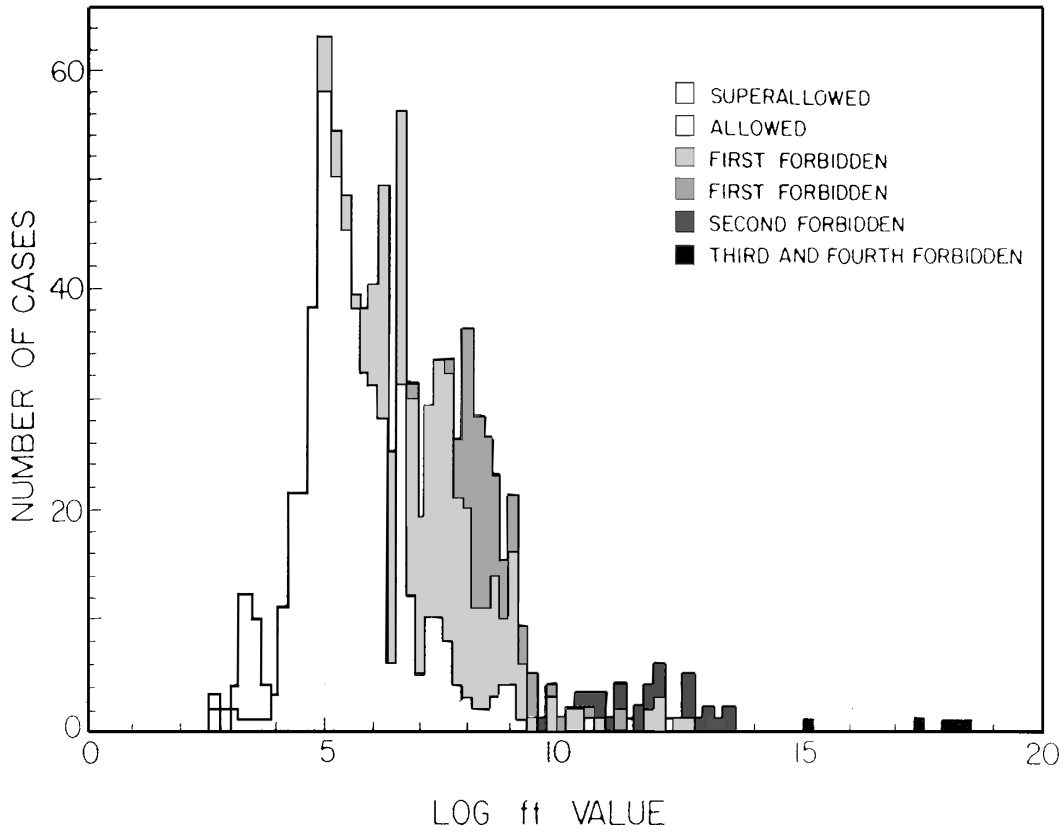


Figure 1 : Systematics of observed log(*ft*)-values for different types of beta-decay. (Adapted from G. E. Gleit et al., *Nucl. Data Sheets* **5** 1963 set 5.) [WO90]

forbidden, etc.

Beta-decay includes three main processes $\beta^-$ (electron emission), $\beta^+$ (positron emission), and EC (electron capture); involving four particles in each interaction - proton, neutron, electron, neutrino, and recently the predicted "bound state beta-decay," with the emitted electron occupying an atomic orbital of the fully stripped ion [JU92] . Each main process of emission is represented by the following:

$\beta^-$ $\qquad Z^A \rightarrow (Z + 1)^A + \beta^- + \bar{\nu}$

$\beta^+$ $\qquad Z^A \rightarrow (Z - 1)^A + \beta^+ + \nu$

EC $\qquad Z^A + e^- \rightarrow (Z - 1)^A + \nu$

As can be seen by the first two interactions, $\beta^-$ and $\beta^+$, energy and momentum are distributed among three particles giving a broad distribution for the beta-particles's energy and momentum.

The beta-decay model proposed by Fermi [FE33] has several observable properties that provide important information about nuclear structure:

1) The beta-energy spectrum shape provides information about angular momentum and parity changes involved in a transition.
2) Coincidence between emitted beta-particles and gamma rays of the daughter nuclei provides information about nuclear level schemes.
3) The definite helicity of the neutrino, see below, implies that the daughter nucleus is polarized [WO90, WU57], allowing for

beta-gamma angular correlation studies.

Another interesting weak interaction property is that parity is not conserved in the decay. In 1956 T.D. Lee and C. N. Yang showed that there was no reason to assume parity conservation in beta-decay; and in 1957 Wu, Ambler, Hayward, Hoppes and Hudson found parity not to be conserved in the decay of $^{60}$Co [HA69, WU57]. Parity non-conservation in weak interactions predict a specific helicity, or longitudinal polarization, of beta-particles. Frauenfelder found longitudinally polarized beta-particles in 1957 with $^{60}$Co. It was later shown that fast moving beta-particles, $\beta^-$, ($v/c \cong 1$) have negative helicity and fast moving beta-positive particles, $\beta^+$, have positive helicity; again verifying that space reflection (parity) is violated [SC66, SE72].

Experiments measuring the correlation between the recoil momentum of the daughter nucleus and the emitted beta-particles have shown the neutrino must have half integral spin [RO55] and negative helicity [GO58, MA58]. These experiments also demonstrated that the best representation for allowed beta-decay is the Vector interaction (V) minus the Axial-vector interaction (A) or V - A theory. Of the five possible interactions, the Pseudoscalar interaction does not contribute in first order to allowed decays. The Scalar and Tensor interactions allow leptons and antileptons to have the same helicity, while the Vector and Axial-vector interactions require these two groups to have opposite helicity [SC66]. Note that in first order, momentum conservation requires that the beta-particle and antineutrino are emitted parallel for the Vector interaction and anti-parallel for the Axial-vector interaction.

This representation of allowed decays by the V - A operator model has been extensively tested. In 1984 A. I. Boothroyd et. al. surveyed the status of experimental results with the standard V - A model of allowed beta-decay. In their review of 92 data values they found that the V - A model with maximal parity violation was compatible

with experimental results [BO84]. They also found that the data did not forbid a small admixture of right-handed lepton currents [BO84].

Since the interaction is represented by a field theory, the complete beta-decay operator is a combination of the beta-neutrino system wave function and the Vector or Axial-vector interaction operators [BL79, RO55, SC66, WO90]. Allowed decays, as stated earlier, are defined to be decays where the beta-neutrino system does not carry away orbital angular momentum, $\Delta l = 0$. Generally the beta-neutrino system wave function is represented by a plane wave of the form $e^{-i\mathbf{k}\cdot\mathbf{r}}$ [BL79, RO55, SC66, WO90]. In lowest order ($kr << 1$, long wave length approximation) the exponential can be replaced by 1 since higher order terms are small and can be neglected. The interaction Hamiltonian for beta-decay contains the following components:

1) Isospin raising or lowering operator, $\boldsymbol{\tau}_{\pm}$.
2) Wave function for the beta-neutrino system, $e^{-i\mathbf{k}\Sigma\mathbf{r}}$ (Equal to **1** for allowed decays).
3) The Axial-vector interaction also contains a spin operator, $\boldsymbol{\sigma}$.

The Vector and Axial-vector interaction are also known as the Fermi and Gamow-Teller interaction, respectively. The Vector interaction or Fermi operator does not have spin coupling and is proportional to **1** and $\boldsymbol{\tau}_{\pm}$. Defining $\Delta J$ as the change in total angular momentum, $\Delta T$ as the change in isospin, $\Delta T_0$ as the change in z-component of isospin, and $\Delta\pi$ as the change in parity between the initial and final nuclear states, the selection rules for a Vector interaction are:

$\Delta J = 0$

$\Delta T = 0$ but $0 \rightarrow 0$ forbidden

$\Delta T_0 = 1$

$\Delta\pi$ = Even

The Axial-vector interaction or Gamow-Teller operator has a spin component and is proportional $\boldsymbol{\sigma}$ and $\boldsymbol{\tau}_{\pm}$. The Axial-vector interaction has the following selection rules:

$\Delta J = 0,1$ but $0 \rightarrow 0$ forbidden

$\Delta T = 0,1$ but $0 \rightarrow 0$ forbidden

$\Delta T_0 = 1$

$\Delta\pi$ = Even

The change in total angular momentum, $\Delta J$, can be 0 or 1 because of the nuclear spin coupling with the beta-neutrino wave function's orbital angular momentum in the Axial-vector interaction. Note that the parity is still even because the beta-neutrino system does not carry away orbital angular momentum, l = 0. A special class of allowed beta-decay, superallowed beta-decay, involve $0^+ \rightarrow 0^+$ transitions. Only the Fermi operator can cause this transition. There is no mixing with the Gamow-Teller operator since no spin coupling is possible [RO55, SC66, WO90].

Up until 1978 the beta-decay interaction was represented by the decay of "bare" nucleons. This means that a neutron decays directly into a proton or vise versa. In 1978 Kubodera, Delorme and Rho proposed that a weak meson exchange current in the nucleus could be observed in the timelike (large energy, small momentum transfer) component in the axial current of beta-decay [KU78]. This meson current could contribute to the observable properties of beta-decay. Extensive investigations by Warburton, Townes and others show that first-forbidden rank zero beta-decays have the best promise for verifying the effects of the meson exchange current in the V - A model [MI82].

## FORBIDDEN BETA DECAY

Forbidden beta-decays are defined by the amount of orbital angular momentum l carried away by the beta-neutrino system. First-forbidden beta-decays involve l=1, second-forbidden beta-decays are l=2, etc. Forbidden beta-decays are further classified by the change in total angular momentum between the nuclear decay states.

Rank 0 $\Delta J = 0$

Rank 1 $\Delta J = 1$

Rank 2 $\Delta J = 2$

The Hamiltonian for forbidden beta-decay thus has terms proportional to $rY_{l,m}(\theta,\phi)$ due to the next higher order terms in the plane wave expansion of the beta-neutrino system. For first-forbidden beta-decay the interaction Hamiltonian is proportional to

$$\boldsymbol{\tau}_{\pm} rY_{l,m}(\theta,\phi) + \boldsymbol{\tau}_{\pm}[\boldsymbol{\sigma} \text{ H } rY_{l}(\theta,\phi)]^{(0,1,2)}$$

giving the following selection rules:

$\Delta J = 0,1,2$

$\Delta T = 0,1$ but $0 \rightarrow 0$ forbidden

$\Delta T_0 = 1$

$\Delta\pi$ = odd [WO90]

Forbidden beta-decays are important because they are predicted to be sensitive

to meson exchange currents in nuclei. In the Vector minus Axial-vector theory, meson exchange currents are believed to enhance the timelike component of the axial-vector current by as much as 40 % over impulse approximations [KU78, MI82, WA91]. This is because the pion has $J^{\pi} = 0^{-}$ as required for first-forbidden beta-decay. First-forbidden rank-zero beta-decays are usually dominated by the Axial-vector operator and therefore they provide a good test for the comparison of theory and experiment [MI82]. Once matrix elements are accurately calculated for rank-zero decays, a further test of the theory is to measure first-forbidden rank-one beta-decay branching ratios to determine the population of higher energy states in the daughter nucleus. One then accounts for contributions from the decay of these higher energy states to the states populated by first-forbidden rank-zero beta-decay. This allows additional refinement in the comparison of theory and experiment.

It should be noted that investigation of forbidden beta-decays also allows other forms of interactions operators. The Pseudoscalar and other induced operators like the induced Tensor interaction may play a role in these decays [SC66]. Improved limits on Scalar interactions could show evidence of this operator [AD93]. Measurements of allowed decays are not sensitive to these induced interactions because the effects of meson exchange currents on allowed operators are very weak and the Pseudoscalar interaction is second order in allowed decays [MI82, AD93]. Therefore, allowed beta-decays are not a sensitive tool to observe these possible effects.

The weak nature of forbidden beta-decays make them a sensitive tool for measuring meson exchange currents, but at the same time also makes them very difficult to measure. Only a few forbidden beta-decays with small branching ratios have been measured for both rank-zero and rank-one decays, as compared to the number of known branching ratios for allowed beta-decays. Branching ratio is defined as the decay probability to the state of interest divided by the total decay probability.

We set out to measure the first-forbidden rank-one beta-decay branching ratios for the transition from the $2^+$ ground state of $^{20}$F to the $3^-$ state at 5.62 MeV and $1^-$ state at 5.79 MeV of $^{20}$Ne. Previous upper limits for these first-forbidden rank-one branching ratios to the $3^-$ and $1^-$ states of $^{20}$Ne are $4.8 \times 10^{-4}$ and $1 \times 10^{-3}$, respectively [AJ78]. The allowed beta-decay branching ratio of $^{20}$F to the $2^+$ state at 1.63 MeV of $^{20}$Ne is 0.9999 [AJ83] and the first-forbidden rank-zero beta-decay branching ratio to the $2^-$ state at 4.97 MeV of $^{20}$Ne is $9.0 \times 10^{-5}$ [AL81a].

# THEORY

## BETA DECAY TRANSITIONS

Fermi's formalism of beta-decay is modeled after electromagnetic interactions with the knowledge that beta-decay is weak and the assumption of a point interaction [FE33]. One obtains Fermi's Golden rule in a straight forward calculation using time dependent perturbation theory with $H(t) = H_0 + H'(t)$. $H_0$ is the time-independent shell model Hamiltonian and $H'(t)$ is the time-dependent interaction Hamiltonian. Expressing the eigenstates of the Hamiltonian H(t) as an expansion of the eigenfunctions of the time independent part of the Hamiltonian, $H_0$:

$$\Psi(\vec{r},t) = \sum_k a_k(t)\Phi_k(\vec{r})e^{-iE_kt/\hbar} \qquad (1)$$

and substituting this representation back into Schrödinger's time-dependent equation one solves for the coefficients $a_k(t)$. The coefficients $a_k(t)$ are probability amplitudes for finding the nucleus in the unperturbed state k at time t. This leads to the relationship

$$|a_k(t)|^2 = 2|\langle\Phi_k(\vec{r})|H'|\Phi_0(\vec{r})\rangle|^2\frac{1 - \cos((E_k - E_0)t/\hbar)}{(E_k - E_0)^2} \qquad (2)$$

$|a_k(t)|^2$ is the probability of finding the nucleus in state k at time t.

Taking the time derivative of equation 2, changing the summation over all possible final states for the daughter nucleus, beta-particle and neutrino to an integration over energy multiplied by the lepton density of final states, and assuming the matrix elements are independent of beta-particle energy one gets Fermi's Golden rule for the total transition probability of allowed beta-decay [BL79, WO90]:

$$\lambda = \frac{2\pi}{S}|\langle \Phi_f(\vec{r})|H'|\Phi_i(\vec{r})\rangle|^2 \rho(E_f)$$

*(3)*

The transition matrix element in equation 3 is also called the shape factor $\mathbf{C}_0$ and the integration over the lepton density of final states, $\rho(E_f)$, is referred to as the allowed Fermi integral $f_0$.

The initial nuclear state in Fermi's Golden rule consists of only the parent nucleus and can be represented by $|J_i M_i \zeta ß$. The final nuclear state consists of the daughter nucleus, emitted beta-particle, and the emitted neutrino. Representing the final nuclear state as $|J_f M_f \xi ß$ and the beta-neutrino system as a plane wave, the transition matrix element in equation 3 can be expanded as shown in equation 4 [WO90]. In equation 4 J is the nuclear angular momentum, M is the nuclear component of angular momentum, $\zeta$ represents all other quantum numbers necessary to uniquely identify the parent nucleus, and $\xi$ represents all other quantum numbers necessary to uniquely identify the daughter nucleus.

$$\langle \Phi_f(\vec{r})|H'|\Phi_i(\vec{r})\rangle = \frac{1}{V}\langle J_f M_f \xi|H' \{\sum_{\lambda=0}^{4}\sum_{\mu=-\lambda}^{\lambda}\sqrt{4\pi(2\lambda+1)}(-i)^{\lambda}(-1)^{\mu} j_\lambda(kr)\, Y_{\lambda\mu}(\theta,\phi)\}|J_i M_i \zeta\rangle$$

*(4)*

$H'$ does not contain any parity changing operators. Keeping only the $\lambda = 0$ term, using the long wave length approximation for the spherical bessel function $j_\lambda(kr)$, summing over all terms, and inserting an explicit beta-decay Hamiltonian for the V - A model [WO90], the transition matrix element for an allowed decay can be expressed as:

$$\langle \Phi_f(\vec{r})|H'|\Phi_i(\vec{r})\rangle =$$

$$\frac{1}{V}\sum_{\kappa M_f}\langle J_f M_f \xi|\sum_{n=1}^{A}\{G_V\tau_{\pm}(n) + G_A\sigma_{\kappa}(n)\tau_{\pm}(n)\}|J_i M_i \zeta\rangle$$

*(5)*

Where $G_V$ if the vector coupling constant and $G_A$ the axial-vector coupling constant.

The parity selection rule for the zero order terms, $\lambda = 0$ in equation 4, describing allowed transitions requires no change in parity [BL55, RO55, WO90]. In our experiment we are interested in the first order terms, $\lambda = 1$ for the beta-neutrino system in equation 4, that describe first-forbidden beta-decays and require a change in parity [BL55, RO55, WO90]. The beta-neutrino system is represented by $Y_{1\mu}(\theta,\phi)$ making the first-forbidden beta-decays proportional to $rY_{1\mu}(\theta,\phi)$ and $(\boldsymbol{\sigma}\mathrm{H}rY_1(\theta,\phi))_{\eta\kappa}$ with $\eta = 0$, 1, and 2. The total spin of the beta-neutrino system is coupled to the intrinsic spin operator $\boldsymbol{\sigma}$, and $\eta$ represents the rank of the spherical tensor operator produced from this coupling indicating the total change in momentum for the transition [WO90]. The transition matrix element for first forbidden beta-decay is

$$\langle \Phi_f(\vec{r})|H'|\Phi_i(\vec{r})\rangle = \frac{1}{V}\sum_{\kappa M_f}\langle J_f M_f \xi|\sum_{n=1}^{A}\{G_V\tau_{\pm}(n) + G_A\sigma_{\kappa}(n)\tau_{\pm}(n)\}$$

$$\times\sum_{\mu=-1}^{1}\{(-i)(-1\ )^{\mu}\sqrt{\frac{4\pi}{3}}(kr)\,Y_{1\mu}(\theta,\phi)\}|J_i M_i \zeta\rangle$$

*(6)*

Since the spherical harmonic $Y_{1\mu}$ has a parity of -1, first forbidden beta-decay has a $\Delta\pi$ = odd. Rank-one beta-decays correspond to a change in the total angular momentum of one unit ($\eta = 1$). The operator $(\boldsymbol{\sigma}\mathrm{H}rY_1(\theta,\phi))_{\eta\kappa}$ is found using the relationship:

$$(\sigma \times rY_1)_{\eta\kappa} = \sum_{m_1 m_2}\langle 1\ m_1\ 1\ m_2 \mid \eta\ \kappa\rangle\sigma_{m_1}\, rY_{1m_2}$$

*(7)*

The terms £1 $m_1$ 1 $m_1$ , η κ ß are Clebsch-Gordan Coefficients.

## COMPARATIVE HALF-LIFE

Correcting beta-decay half-lives $t_{1/2}$ for the decay energy and charge of the daughter nucleus results in values that are comparative for decays with similar characteristics [FE33]. These corrected half-lives are called comparative half-lives and are represented in the literature as *ft* values. The factor *f* is called the Fermi integral. There is a large spread in the *ft* values; however, the log(*ft*) does show some grouping within each class of decays, see figure 1.

The Fermi integral is defined using Fermi's Golden Rule. In its development above we approximated that the transitions matrix elements were independent of the beta-particle energy. This is true for allowed beta-decays since the first term of the bessel function contained in our plane wave expansion is 1. Since the transition matrix elements for allowed beta-decays are independent of energy, they are taken outside the integral over the allowed density of states. Substituting the expression for the density of states and integrating over all final beta-particle momenta, one obtains the definition for the Fermi integral. Using this approximation the Fermi integral for allowed beta-decay is:

$$f_0 = \int_{?}^{?} F(Z, E_e)\left(\frac{p_e}{m_e c}\right)^2\left(\frac{E_0 - E_e}{m_e c^2}\right)^2\left(\frac{dp_e}{m_e c}\right) \qquad (8)$$

The Fermi function $F(Z,E_e)$ corrects the beta-state density for distortion effects caused by the nuclear charge Z of the daughter nucleus and beta-particle energy $E_e$ [BL79, SC66, WO90]. The term $E_0$ is the beta-particle end point energy for the transition. Expressing the transition probability as a function of the Fermi integral for allowed beta-decay:

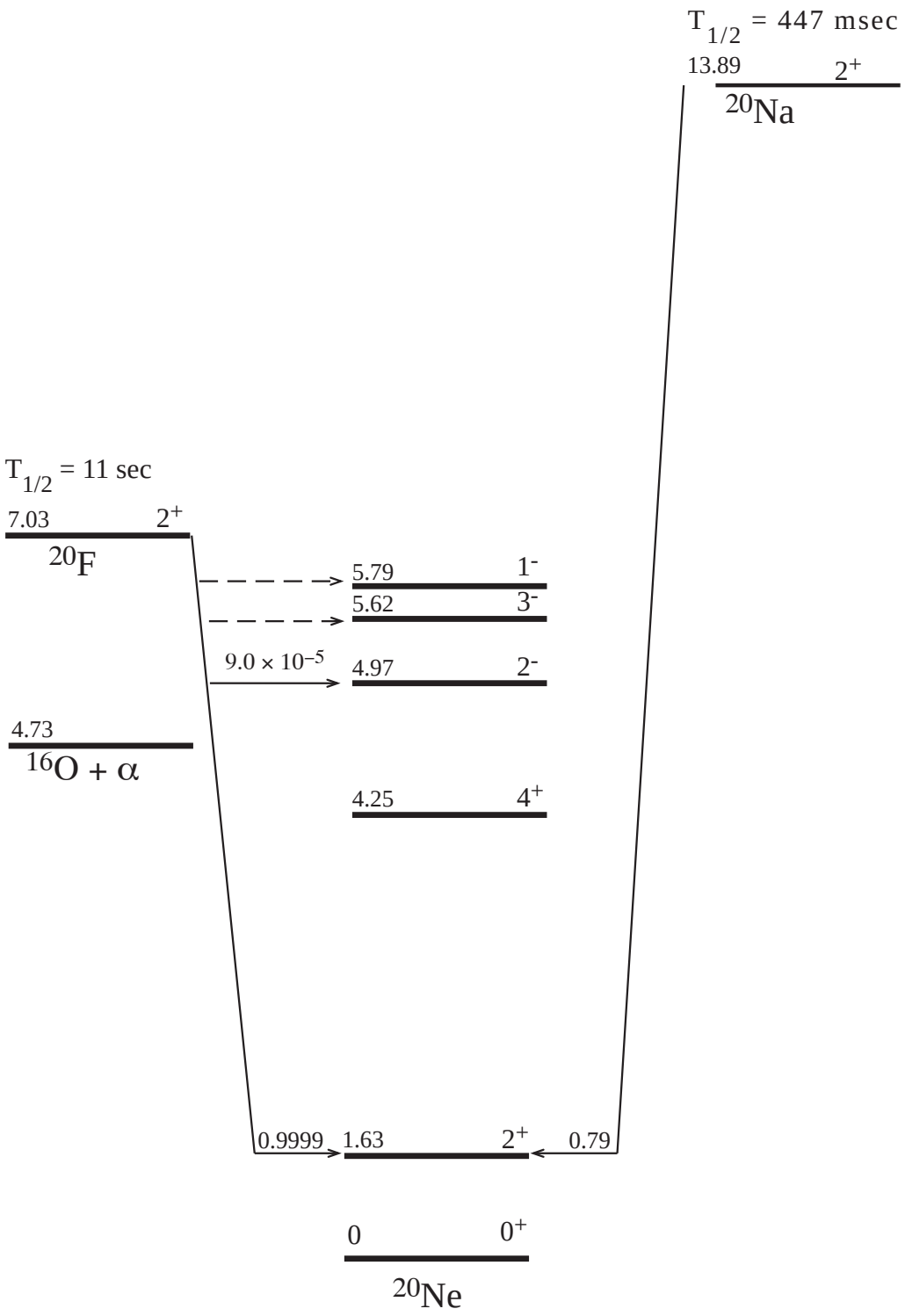


Figure 2 : Energy level diagram of $^{20}$Ne [AJ83].

$$\lambda = \frac{\ln 2}{t_{1/2}} = \frac{m_e^5 c^4}{2\pi^3 S^7} f_0 \, |\langle \Phi_k(\vec{r}) | H' | \Phi_0(\vec{r}) \rangle|^2$$

*(9)*

The Fermi integral cannot be expressed in a simple form if the transition matrix elements depend on beta-particle energy. This is the situation for forbidden beta-decay since the operators in the perturbed Hamiltonian H′ are dependent on the beta-particle energy. Because one does not know the correct functional relationships for the beta-neutrino system, the nuclear wave functions, or the beta-decay operators, the Fermi integral in forbidden decays must be approximated. In forbidden beta-decay it is customary to calculate the Fermi integral as if the beta-decay was allowed and approximate the transition matrix elements or shape factor **C**. Using experimental results one then estimates the transition matrix elements from the relationship.

$$\lambda \propto f_0 \, |\langle \Phi_f(\vec{r}) | H' | \Phi_i(\vec{r}) \rangle|^2$$

*(10)*

The transition probability for beta-decay is proportional to the square of the nuclear matrix element multiplied by the Fermi integral or beta-neutrino system phase-space factor [BL79, WO90]. This relationship allows the use of the known branching ratio for the first-forbidden rank-zero beta-decay from the $2^+$ ground state of $^{20}F$ to the $2^-$ lowest excited state of $^{20}Ne$ at 1.63 MeV, BR = 9.0(4) x $10^{-5}$ [AL81a] see figure 2, to estimate the first-forbidden rank-one beta-decay branching ratios to the $3^-$ and $1^-$ lowest excited states of $^{20}Ne$, at 5.62 MeV and 5.79 MeV, respectively. It is known that the Fermi integral or phase-space factor is proportional to the total nuclear transition energy raised to the fifth power [BL79, SC66, WO90]. Applying this energy correction to the first-forbidden rank-zero beta-decay branching ratio, the first-forbidden rank-one beta-decay branching ratios to the lowest $3^-$ and $1^-$ states are estimated to be 1.4 x $10^{-5}$ and 7 x $10^{-6}$,

respectively. Through systematic studies of beta decay, E. K. Warburton proposed that the square of the nuclear matrix elements for first-forbidden rank-zero beta-decays are larger by approximately a factor of 10 than first-forbidden rank-one beta-decays (Private communication to Moshe Gai, 1992). Application of this proposal and the energy correction to the known first-forbidden rank-zero beta-decay branching ratio results in estimates for the first-forbidden rank-one beta-decay branching ratios to the $3^-$ and $1^-$ states of $^{20}$Ne to be $1.4 \times 10^{-6}$ and $7 \times 10^{-7}$, respectively.

## Meson Exchange Currents

It has been proposed that meson exchange currents (mec) dominated by soft pion (large E, small $|\vec{p}|$) exchange in the nucleus significantly enhance the timelike component of the axial current [KU78, RI90]. Analysis of this possible enhancement of the timelike component in weak axial currents predict that first-forbidden transitions show the greatest promise in revealing this effect [TO86, WA91, WA94]. Since the timelike component of the axial current operator dominates first-forbidden rank-zero beta-decays [GU78, KU78, WA91], and the pion possess the correct quantum number $J^\pi = 0^-$ for first-forbidden rank-zero beta-decay, these decays provide information on a possible coupling. First-forbidden beta-decays therefore allow the study of subnucleonic degrees of freedom in nuclei. The verification of this process is very difficult because the choice of basis functions used for nuclear wave functions influence the calculations and forbidden transitions are not easily measurable [TO86a, TO86].

First-forbidden rank-one beta-decays play an important role in verifying meson exchange current enhancements since accurate measurements of these decays allow the removal of measurable contributions to rank-zero decays. Removing the effects of the decay of higher energy states populated by rank-one beta-decay that subsequently decay to states populated by rank-zero beta-decay allows for an improved measurement. It is

also important to estimate the effect of rank-one beta moments on first-forbidden rank-zero beta-decays. In a rank-zero decay the transition matrix elements consist of rank-zero, rank-one, and rank-two operators. Accurately measuring the effects of rank-one operators improve the estimates for meson exchange currents in nuclei. A shell-model study of eighteen first-forbidden beta-decays in the lead region showed the importance of understanding the rank-one component to rank-zero decays [WO91]. In the small atomic number region, A=16, calculations of first-forbidden rank-zero beta-decays are approximated without contributions from rank-one operators [WA94]. Measuring first-forbidden rank-one beta-decay branching ratios in this region will allow for an improved test of theory and experiment by taking into account the effects of rank-one operators on rank-zero decays.

# THE EXPERIMENT

## TARGET DEVELOPMENT

For target development it was advantageous to consider a target that could be used both in this experiment and in a concurrent experiment on the Beta-Delayed Alpha-Decay of $^{16}N$. The target requirements for both the $^{20}F$ and $^{16}N$ experiments were very similiar and required targets that produced:

1) Good cross sections for neutron capture by the beams, $^{19}F$ and $^{15}N$.
2) Minimal angular distribution of the secondary beams of $^{20}F$ and $^{16}N$ in the laboratory frame of reference.
3) Minimal background in the regions of interest for the alpha-particle decays.

If a common target could be developed it would enable greater flexibility in the conversion of the experimental apparatus to measure these two decays concurrently.

The first consideration for a target was a deposit of deuterided metals on a thin carbon foil. This type of target was considered because of its success in Z. Zhao thesis work on the Beta-Delayed Alpha-Decay of $^{16}N$ [ZH92]. After careful investigation it was determined that the melting points and decomposition temperatures were too low to be useful due to the heat produced by the large beam currents we are forced to use [HU52, LE67, SH67, SP61].

Mr. R. H. France III developed a deuterium gas target for his Ph.D. thesis on $^{16}N$ that could also be used for the study of $^{20}F$ decay and other experiments [FR96]. Computer simulations of $^{20}F$ multiple scattering in 1mg/cm$^2$ Beryllium, the gas target windows, at 40 MeV using TRIM 92 showed that the beam remained collimated to within 1 degree of its

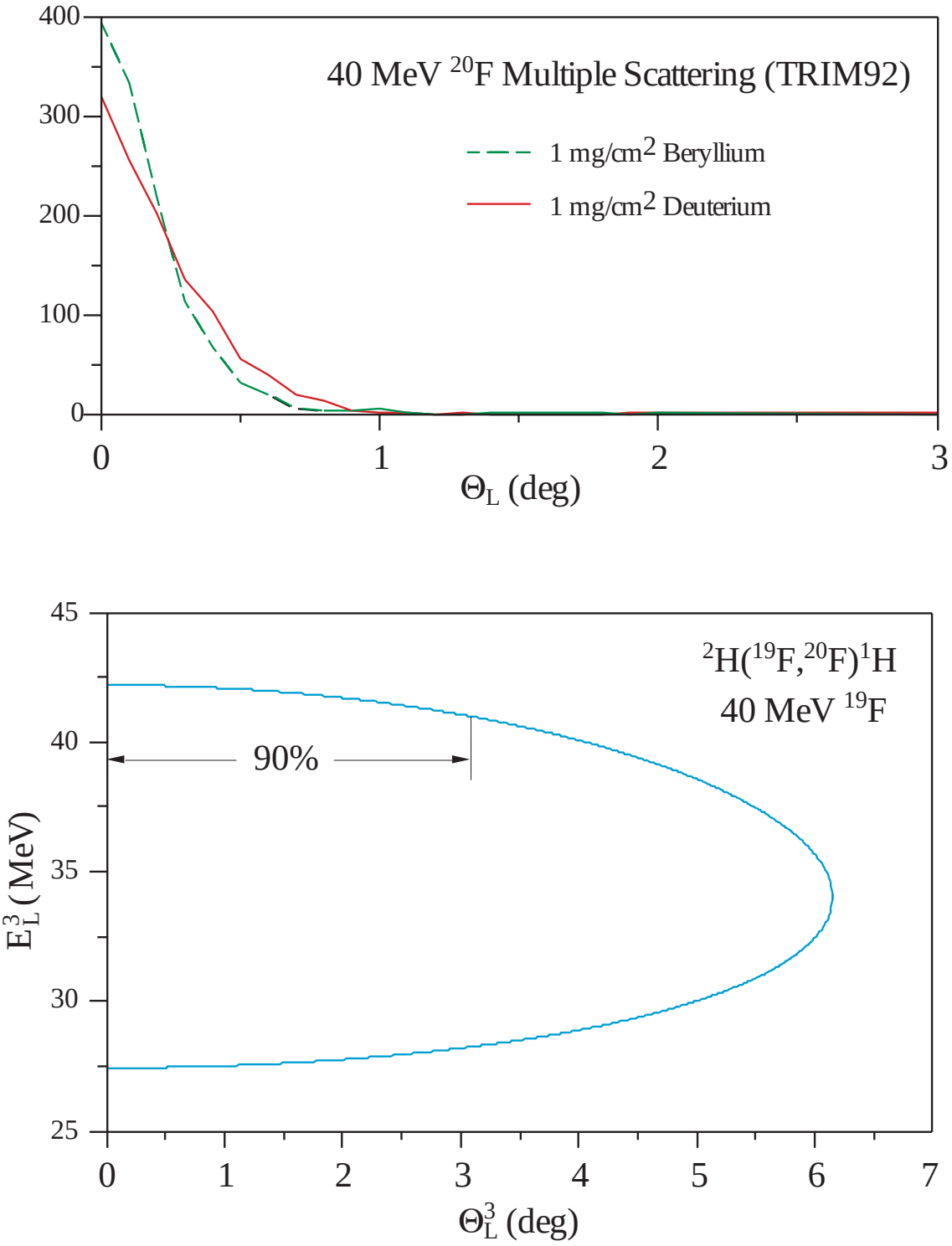


Figure 3 : Top - Typical plot of multiple scattering of $^{20}F$ in $^{9}Be$ and $^{2}H$. Bottom - Typical kinematics plot of $^{2}H(^{19}F,^{20}F)^{1}H$ reaction.

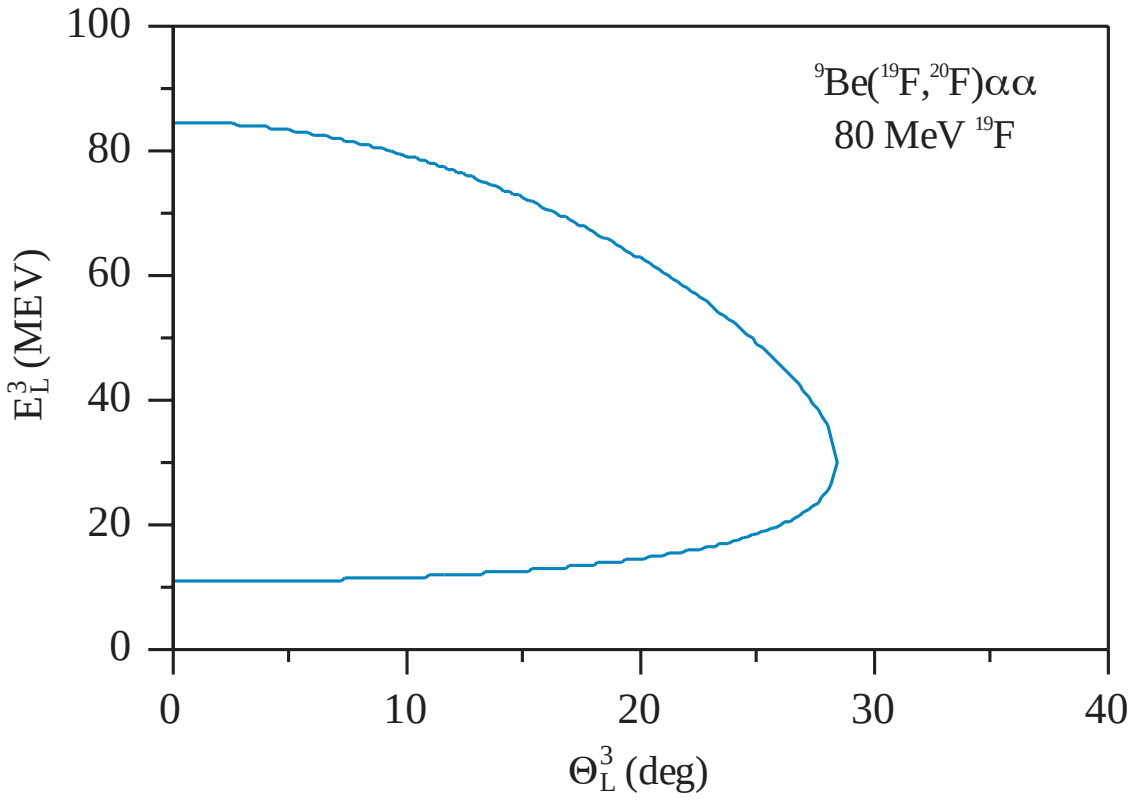


Figure 4 : Typical kinematics plot of $^9$Be($^{19}$F,$^{20}$F)αα reaction.

original direction in the lab reference frame, see figure 3 [ZI91]. Kinematic calculations of the production of $^{20}F$ at 40 MeV with the reaction $^{2}H(^{19}F,^{20}F)^{1}H$ also showed that 90% of the reaction products were within $3^{o}$ of the initial beam direction, see figure 3. These computer simulations predicted that a gas target with $^{9}Be$ windows would produce a well collimated quasi mono-energetic secondary beam of $^{20}F$.

The deuterium gas target proved to be unsuccessful for this experiment due to the significant neutron induced background produced. The neutron induced background overwhelmed the region of interest in the alpha-energy spectrum limiting the sensitivity to low energy alpha-particles emitted from the $1^{-}$ state in $^{20}Ne$ at 5.79 MeV and $3^{-}$ state in $^{20}Ne$ at 5.62 MeV, with predicted energies of 0.85 MeV and 0.71 MeV, respectively.

Through the testing of the deuterium gas target it became apparent that a solid $^{9}Be$ target (i.e. the exit foil of the gas target alone) would be useful in measuring first-forbidden rank-one beta-decays of $^{20}F$. The $^{9}Be(^{18}O,^{19}O)\alpha\alpha$ reaction was demonstrated to have a high relative yield of radioactive nuclides in beta-decay measurements [AL81]. Testing of this target showed that:

1) Its neutron induced background was significantly reduced.
2) It could withstand the beam currents necessary to produce the large number of $^{20}F$ nuclei necessary to measure the first-forbidden rank-one beta-decays, see figure 5.

A computer simulation for the target used in this experiment predicted results similar to the gas target for multiple scattering of a secondary beam of 80 MeV $^{20}F$ on a 0.0025 cm thick Be target at $60^{o}$ to the beam, see figure 6 [ZI91]. However, the kinematics of the $^{9}Be(^{19}F,^{20}F)\alpha\alpha$ exit channel predicted an increase in the laboratory frame of reference's $^{20}F$ maximum angular distribution, see figure 4. An additional collimator was placed in the

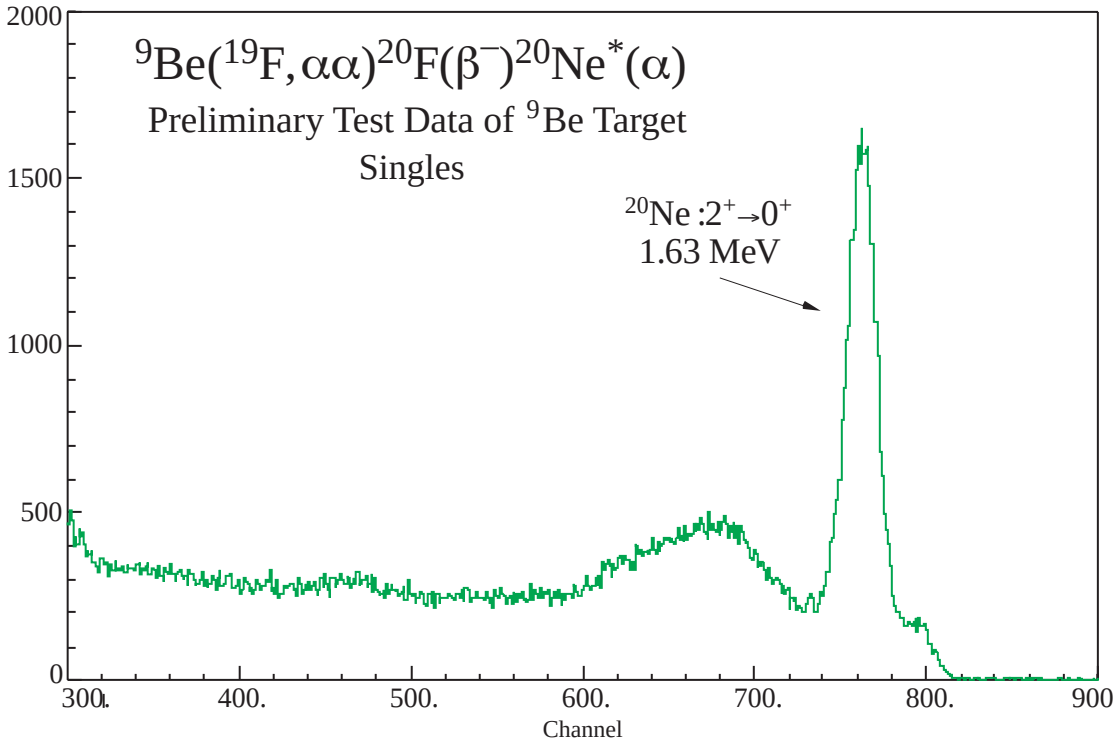


Figure 5 : Preliminary test data for $^{9}$Be solid target.

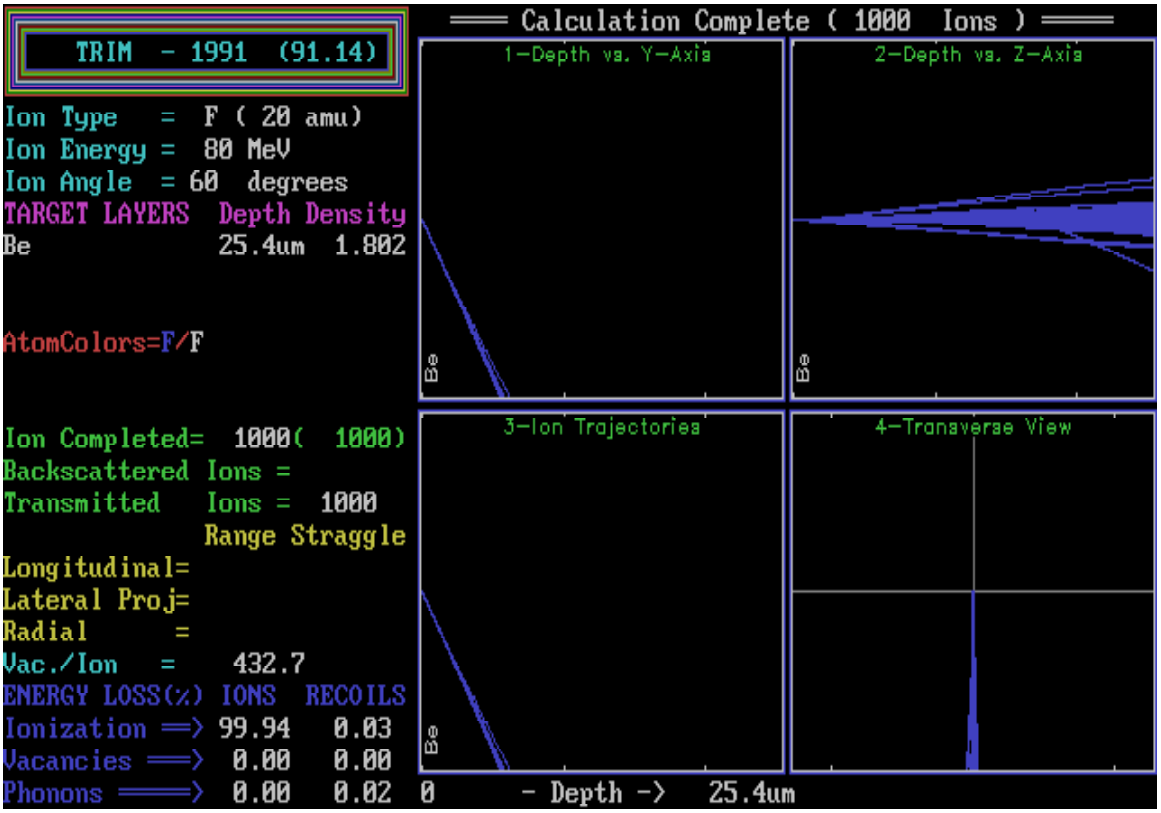


Figure 6 : Typical range and straggling calculation for transmitted $^{20}$F nuclei in beryllium target at 60$^{o}$ incident angle and 80 MeV initial energy. Secondary beam of $^{20}$F remains collimated to within 1$^{o}$ of $^{19}$F beam's original direction in the lab reference frame.

beam to minimize the background caused by deposited $^{20}F$ on the internal chamber components due to the increased angular distribution of $^{20}F$.

## Experimental Procedures

The energy level structure of $^{20}Ne$ in relation to the ground state of $^{20}F$ makes $^{20}F$ a good candidate for measuring the branching ratio of a first-forbidden rank-one beta-decay. In this decay the lowest $3^-$ and $1^-$ excited states, at 5.62 MeV and 5.79 MeV, respectively, of $^{20}Ne$ are above the $^{16}O + \alpha$ threshold at 4.73 MeV, see figure 2. Since both the lowest $3^-$ and $1^-$ excited states in $^{20}Ne$ decay primarily (larger than 92%,99% respectively) through alpha-particle emission [AJ87], this allows the use beta-delayed alpha-decay to minimize the background in the first-forbidden rank-one beta-decay branching ratio measurements.

The low background and high sensitivity obtained in this experiment is based on coincidence measurements between beta-particles and alpha-particles from forbidden beta-decays of $^{20}F$. These alpha-decays are normalized to the gamma-decay of the $2^+$ excited state at 1.63 MeV in $^{20}Ne$ in coincidence with the beta-particles emitted from the allowed beta-decay of $^{20}F$. This allowed beta-decay is measured to have a branching ratio of 99.99%. A comparison of the decays of the $2^+$ first excited state at 1.63 MeV in $^{20}Ne$ with the lowest excited $1^-$ and $3^-$ states at 5.79 MeV and 5.62 MeV, respectively, in $^{20}Ne$ yields the absolute normalization of the branching ratios for the first-forbidden rank-one beta-decays. Since the branching ratios were estimated to be on the order of $10^{-5}$ to $10^{-6}$, minimizing the background is essential for increasing sensitivity while at the same time maintaining a reasonable production of $^{20}F$. These two conditions played a major role in the design of the experiment.

We produced $^{20}F$ using the reaction $^{9}Be(^{19}F,^{20}F)\alpha\alpha$. A $^{19}F$ beam was chosen with a $^{9}Be$ solid target so as to increase the production of $^{20}F$. The $^{19}F$ beam was accelerated to an

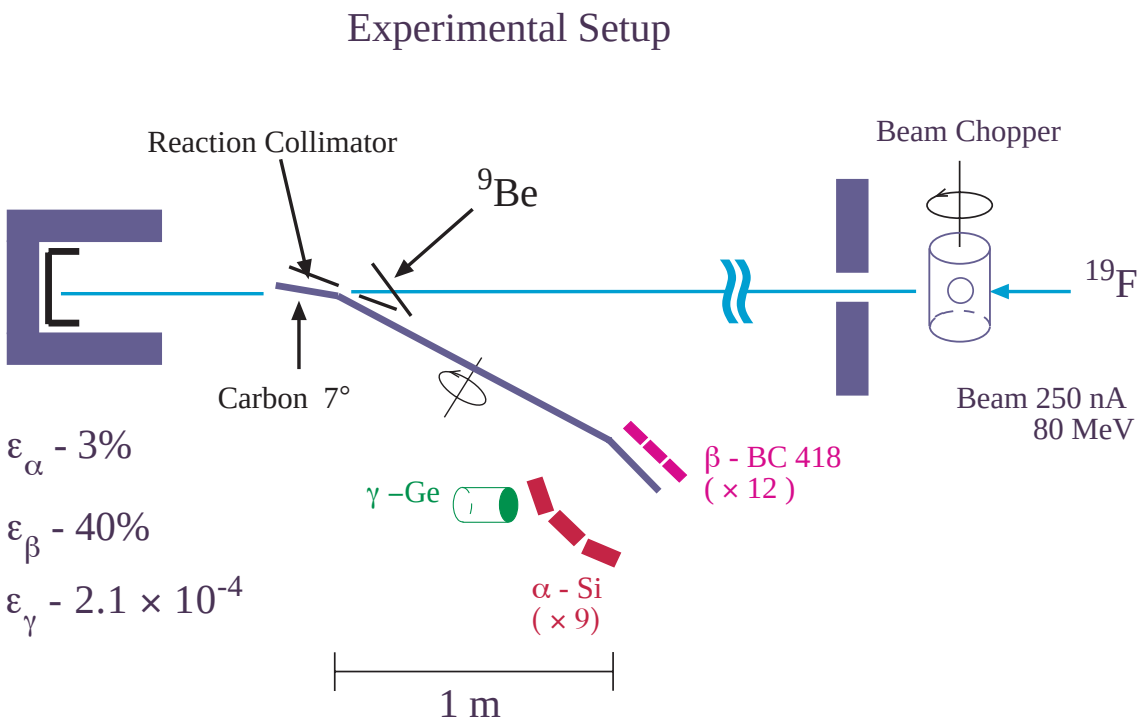


Figure 7 : Experimental setup used in current measurement.

energy of 80 MeV using the ESTU tandem accelerator at Yale University's Wright Nuclear Structure Lab (WNSL). A 80 MeV $^{19}F$ beam was collimated and sent to a production area just inside the vacuum chamber. Here the $^{19}F$ beam hit a $^{9}Be$ solid target that was at an angle of approximately $25^{o}$ to the beam producing $^{20}F$. The kinematics of a $^{19}F$ beam on a $^{9}Be$ solid target allowed us to produce a $^{20}F$ beam as discussed above, see figure 4. The reaction products then passed through a rectangular collimator to reduce background by shielding a catcher foil frame and allowing the $^{20}F$ produced to be deposited only on a thin carbon catcher foil and not on the frame holding the foil. The catcher foil consisted of a $30\mu g/cm^2$ thick carbon foil mounted on a rotating arm and frame assembly. The catcher foil was mounted at an angle of approximately $7^{o}$ with respect to the beam, see figure 7. This orientation produced an effective catcher foil thickness 8 times greater than its actual thickness. Placement of a thin foil in this manner allows the use of a thin catcher foil to efficiently collect reaction products.

The accelerated beam was chopped at the accelerator vault, approximately 30 meters from the target. After the beam was on for 16 seconds, the catcher foil and arm were then rotated with the chopper in. An electronic monitoring system ensured that the beam was chopped before the arm was rotated to prevent spraying reaction products on the catcher arm frame. The rotation of the catcher foil to the counting area took approximately 3 seconds to allow the decay of short lived contaminates. All detectors were inhibited from collecting information using both hardware and software conditions during the arm's rotation. This minimized background caused by electrical noise produced during the arm's rotation. Once sensors indicated that the catcher foil was rotated to its proper location, data collection proceeded for approximately 13 seconds. See figures 8, 9, and 10 for typical control room electrical schematics.

The faces of the alpha-array and beta-array were placed on opposite sides and parallel to the catcher foil to maximize the counting efficiency of each array, see figure 7. In this

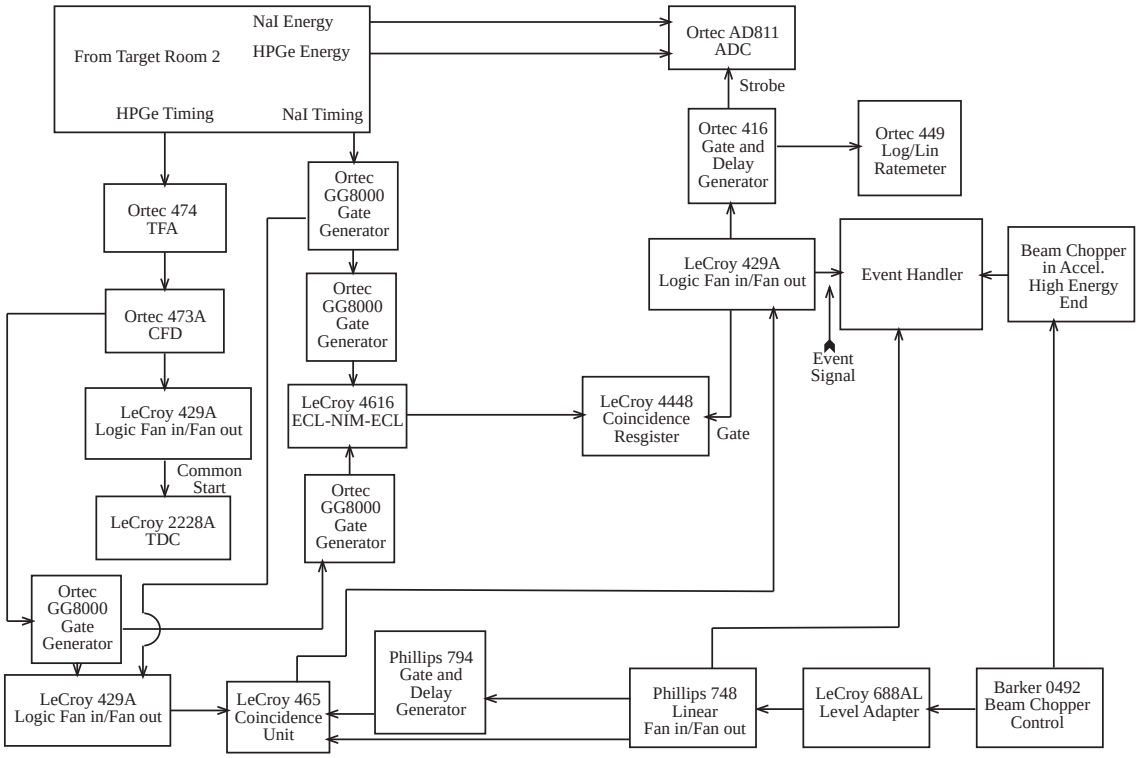


Figure 8 : Typical gamma-ray detector electronics placed in WNSL control room.

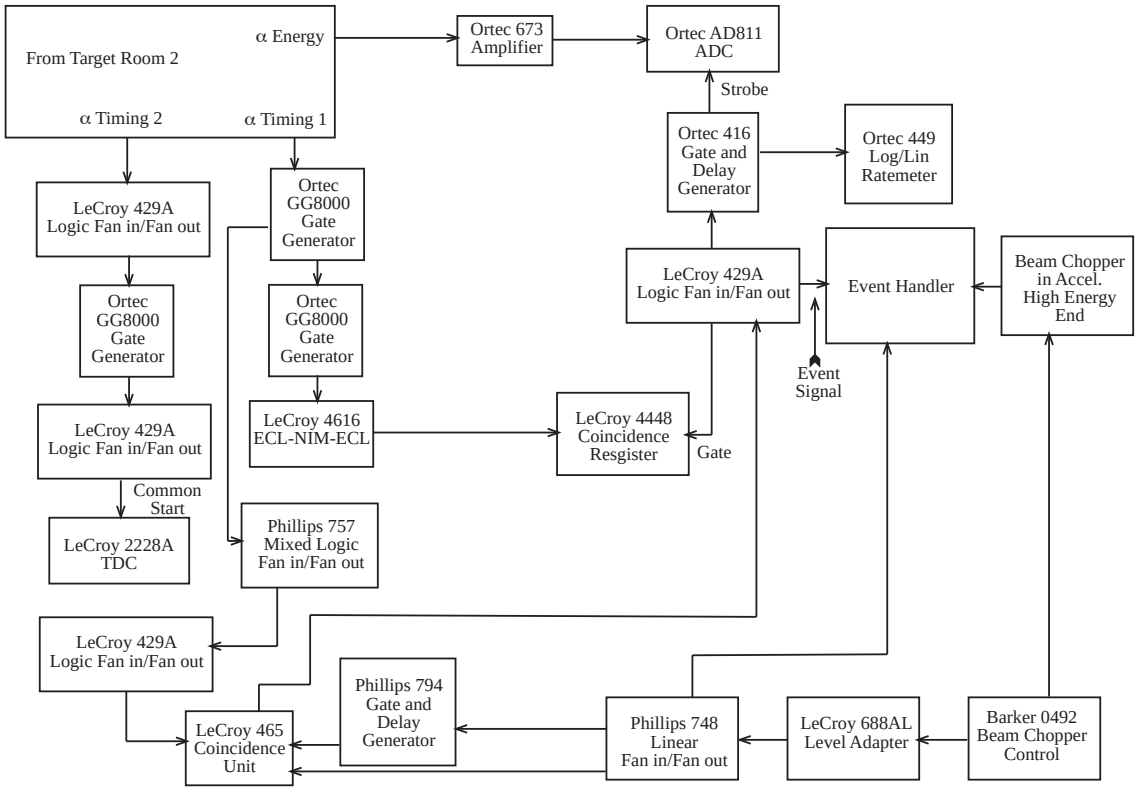


Figure 9 : Typical alpha-detector electronics placed in WNSL control room.

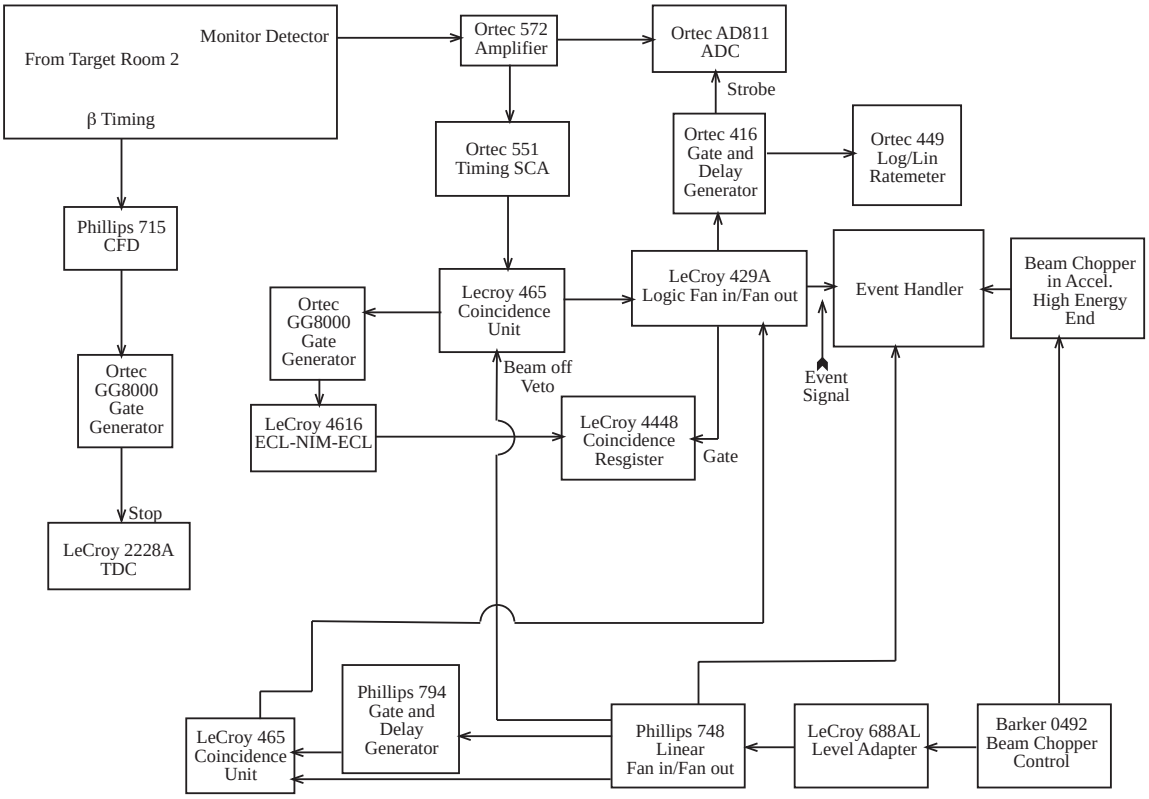


Figure 10 : Typical beta-particle and monitor detector electronics placed in WNSL control room.

position the catcher foils appear very thin to the alpha-particles detectable by the alpha-array that emerged essentially perpendicular to the catcher foil minimizing alpha-particle energy loss in the foil. This must be achieved as the alpha-particles emitted from the $3^-$ state have an energy of 710 keV and from the $1^-$ state 850 keV. The experimental challenge was balancing the need for a thick catcher foil to maximize the collection of $^{20}$F with the need for a very thin foil to minimize alpha-particle energy loss. Indeed, the 30 $\mu g/cm^2$ carbon catcher foil tilted at $7^o$ to beam provided a satisfactory solution.

The alpha-array consisted of nine silicon surface barrier detectors each having an active area of 450 $mm^2$ and 50$\mu$m thick. The electronic threshold for each detector was set typically at 200 keV. The alpha-array was located approximately 69mm from the catcher foil to ensure good energy resolution, minimize background, increase the alpha-particle time-of-flight to the detector, and to minimize dead time caused by the event rate in the alpha-array. The catcher foil energy resolution was approximately 30 keV. The total array absolute efficiency was measured to be 2.69(1)% with an energy resolution of 73.5 keV FWHM.

Two detectors were used to measure the gamma-emission, a high resolution HPGe detector and NaI(Tl) detector. The HPGe and NaI(Tl) detectors were located 37 cm from the catcher foil at an angle that allowed them to view the catcher foil without being blocked by the alpha-array. At this distance, the HPGe detector had an efficiency of 2.1(3) x $10^{-4}$ for the 1.63 MeV gamma-ray and 1.6(3) x $10^{-4}$ for the 3.33 MeV gamma-ray emitted from the $2^+$ and $2^-$ states in $^{20}$Ne, respectively, populated by the beta-decay of $^{20}$F. This detector could in principle be placed at any angle to the catcher foil since the gamma-rays from the $2^+$ at 1.63 MeV are emitted isotropicly. Also, the beta-array high geometrical efficiency of 40% and large angular coverage removes any concerns arising from alignment of nuclear states (beta-gamma angular correlation).

The beta-array consisted of twelve BC418 plastic scintillator detectors inside the

vacuum chamber that were optically coupled to photomultiplier tubes outside the vacuum chamber. Electronic threshold of each beta detector was set typically at 80 keV. This array was located within 3 mm of the catcher foil when it was in its counting position. Since we only needed to know when a beta-particle was detected in this array for coincidence information, no energy information was recorded. The plastic scintillator timing signal was used to stop the coincidence counting so as to minimize dead time. With the catcher foil located in approximately the center of this array, the beta-efficiency was measured to be approximately 40% with a time resolution of 4 nanoseconds for alpha-energy of 5.8 MeV. Timing resolution for alpha-beta coincidence was on the order of 4 nanoseconds due to the very low threshold and large capacitance of Si-detectors. Long rise times of the HPGe detector timing pulse yielded time resolution for gamma-beta coincidence on the order of 20 nanoseconds. The obtained timing resolutions were sufficient to remove a significant amount of background in the alpha-particle and gamma-ray spectrums.

The presence of an event in either the alpha-detector array or HPGe detector was used to trigger the processing of information from all detectors. A delay between the output of the beta-array detectors ensured that true signals from this array came after the alpha-array or HPGe detectors even though beta-particles precede both the alpha- and gamma-decays. Starting the events on the lower rate alpha-particle or gamma-ray reduces the event rate of the electronic system and minimizes dead time, while at the same time it allows the collection of real events, see figures 8, 9, and 10.

We recorded the following parameters for each decay:

1) Energy deposited in SSB detector in the alpha-array.
2) Gamma ray energy.
3) Timing between the start of an event by an alpha-particle or gamma-ray detector and detection of a beta-particle in one of the

beta-array detectors.

4) The latch identification of each detector in the alpha-array, monitor detector, the HPGe detector, and NaI(Tl) detector that processed a signal meeting threshold criteria.

This detailed record of each parameter allows the analysis of various data with gating on specific conditions. The data were analyzed off line by placing gates and conditions on the above recorded information.

After a counting time of 13 seconds, the detectors in the counting area were inhibited and the beam chopper opened allowing the beam to hit the $^{9}$Be target producing $^{20}$F. Two 30μg/cm$^2$ catcher foils were used, utilizing both ends of the rotating arm, see figure 7. We collected $^{20}$F on a catcher foil for 16 seconds, stopped the beam, rotated the arm (3 second duration), and collected data for 13 seconds repeating the complete cycle. This sequence gave beam on and beam off times of 16 seconds each. The beam chopper, rotating arm, and data collection were controlled by the Concurrent Computer system at WNSL allowing for continuous operation and data collection.

The total beam current was monitored using Rutherford backscattering of $^{19}$F from a 30μg/cm$^2$ gold on 30μg/cm$^2$ carbon target. A silicon surface barrier detector placed 7 cm from this foil at a backward angle of 140$^{o}$ to the beam direction was used to measure the $^{19}$F beam current. This detector was active while the beam was on and the arm stationary. This allowed normalization of background runs without the catcher foils to data collection runs, enabling us to perform an effective background subtraction.

## Experimental Results

Figure 11 shows the energy spectrum of the alpha-decay of $^{20}$Ne in singles with a tail

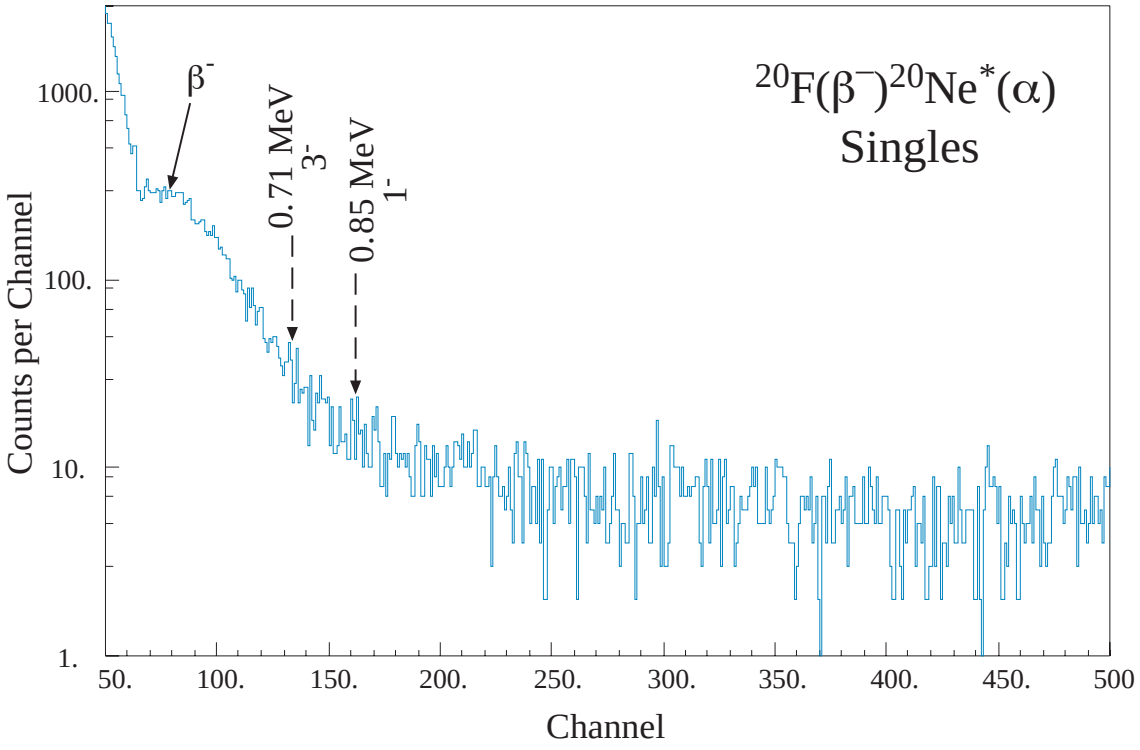


Figure 11 : Alpha-particle spectrum in singles. Energy calibration corrected for 30 μg/cm$^2$ carbon catcher foil is E = (0.0049 MeV/Ch) (Ch. #) + 0.049 MeV.

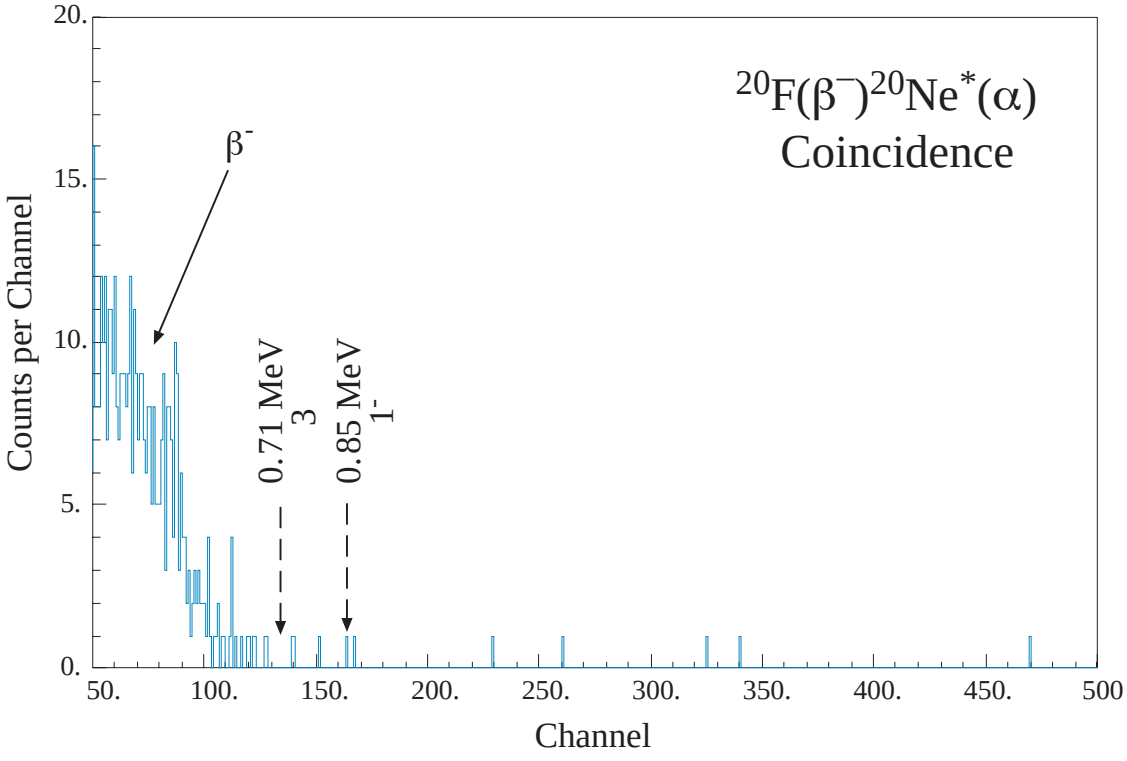


Figure 12 : Alpha-particle spectrum in fast (Δt = 20 nsec) coincidence with beta-particles. Energy calibration corrected for 30 μg/cm$^2$ carbon catcher foil is
E = (0.0049 MeV/Ch) (Ch. #) + 0.049 MeV.

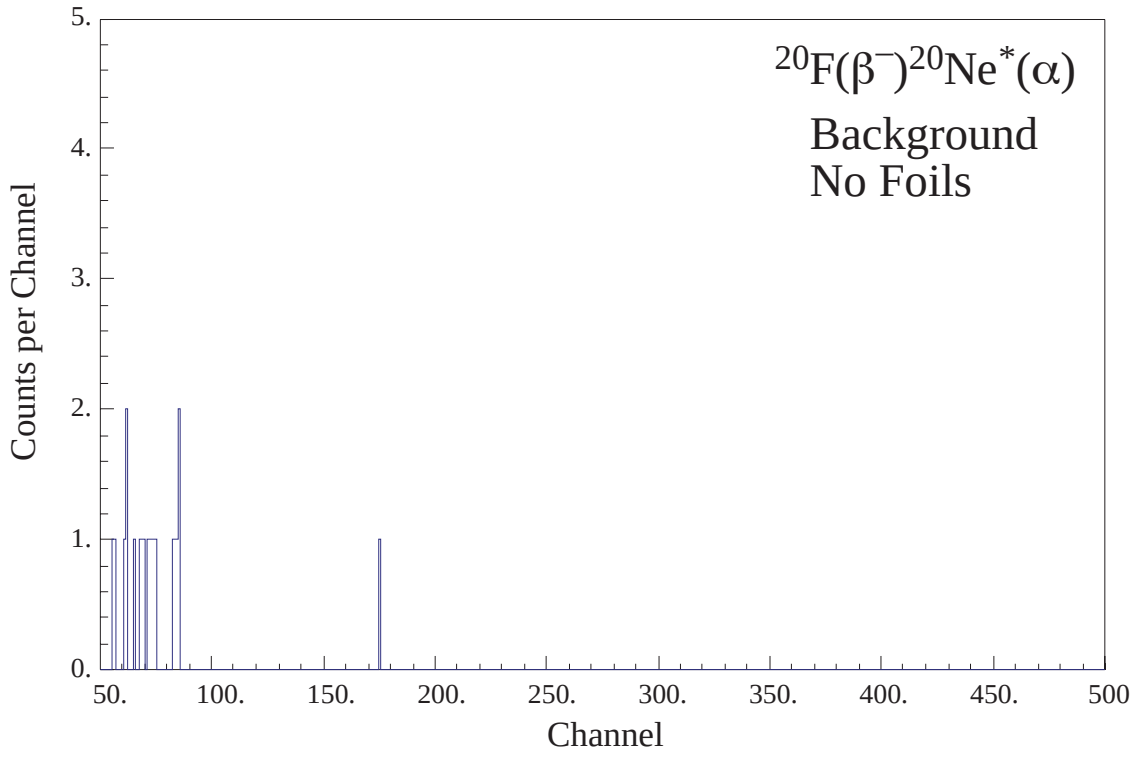


Figure 13 : Background alpha-particle spectrum in coincidence with beta-decay of $^{20}F$ without carbon catcher foils.

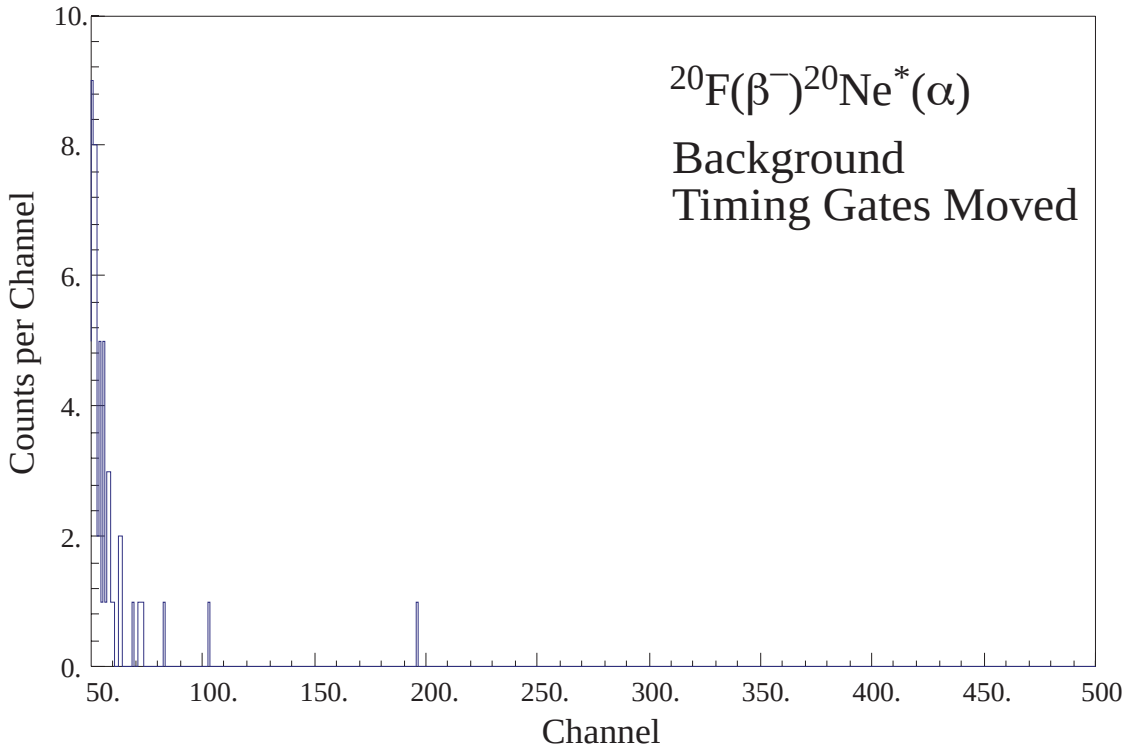


Figure 14 : Background alpha-particle spectrum in coincidence with beta-decay of $^{20}F$ - timing gates shifted 20 nsec to allow random coincidence.

from beta-particles. The two methods used to estimate the first-forbidden rank-one beta-decay branching ratios predict 150 counts for a phase space correction to the first-forbidden rank-zero branching ratio and 15 counts with Warburton's proposed nuclear matrix element reduction in an energy range of 157 keV (32 Channels) for the alpha-decay of the $3^-$ state. These methods predict 80 counts and 8 counts, respectively, for the alpha-decay of the $1^-$ state of $^{20}$Ne. The regions of interest for the alpha-decay of the $3^-$ state and $1^-$ state in $^{20}$Ne have 1071 and 510 background counts, respectively, thus giving an expected signal to background worse than 1 to 6. This required a reduction in the background to measure the first-forbidden rank-one beta-decay of $^{20}$F, accomplished by gating the alpha-particle spectrum on the coincidence between the beta-particle and the subsequent alpha-particle decay.

Figure 12 shows the alpha-particle detector energy spectrum in coincidence with beta-particles. In this spectrum there are a total of seven counts in the region of interest, 0.64 MeV to 0.79 MeV (channels 120 to 152), for the alpha-decay of the $3^-$ state and a total of three counts in the region of interest, 0.77 MeV to 0.93 MeV (channels 148 to 180), for the alpha-decay of the $1^-$ state of $^{20}$Ne. We determined the background for the alpha-particle spectrum in coincidence with beta-particles by removing the carbon catcher foils and gating on the same conditions used for data analysis. This measures the background due to the spraying of $^{20}$F reaction products on the catcher foil frames. We also measured background by shifting the timing gates to allow the subtraction of random coincidence events. Figures 13 and 14 shows the alpha-particle background spectrums. These spectrums demonstrate that the catcher foil frames were sufficiently shielded to prevent the spraying of a significant amount of $^{20}$F on them.

The alpha-detector array was calibrated using several different alpha-particle sources. Energy calibration in the region of interest was preformed using the reactions $^{10}B(n,\alpha)^7Li$ and $^{10}B(n,\alpha)^7Li^*$ to first exited state [KN89]. The reactions produced 0.841 MeV and 1.014 MeV $^7$Li particles, and 1.471 MeV and 1.775 MeV alpha-particles, see figure 15. In addition,

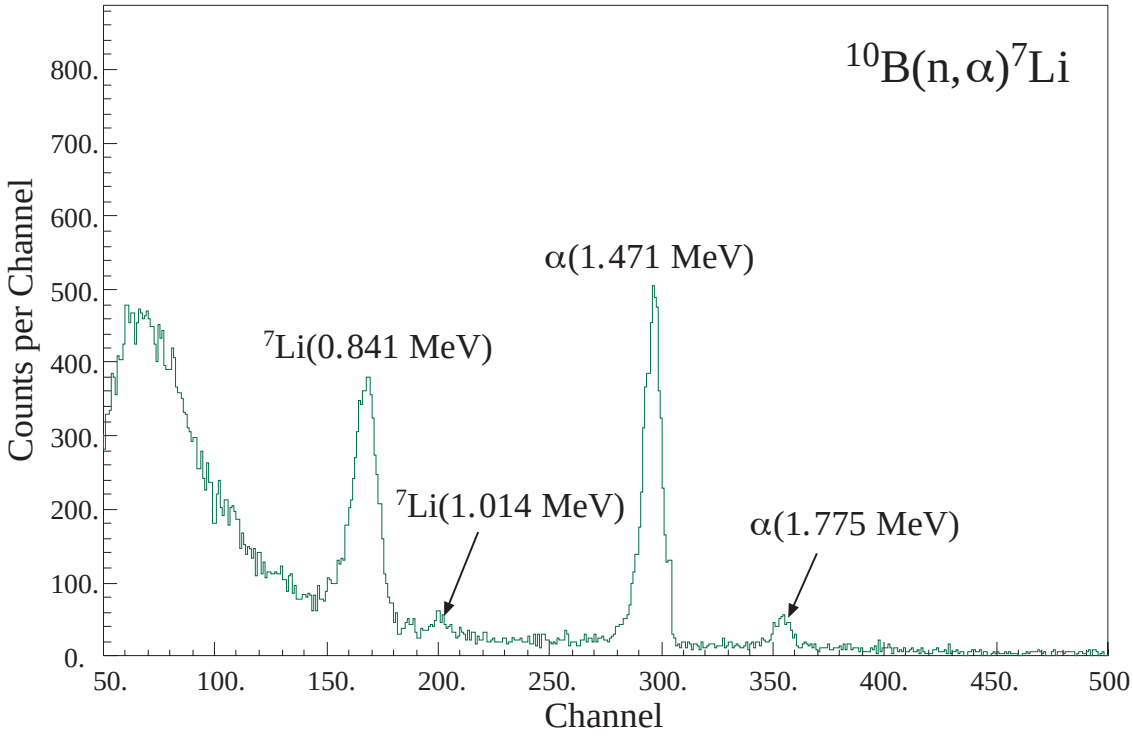


Figure 15 : Typical charged particle energy calibration spectrum from $^{10}B(n,\alpha)^{7}Li^{(*)}$ reaction. Thermalized neutrons from a Pu-Be neutron source reacted with isotopically enriched $^{10}B_2O_3$ targets.

standard calibration sources of $^{148}$Gd, $^{241}$Am, $^{208}$Po and $^{209}$Po were used for energy calibration of the alpha-detector array. The absolute efficiency of the alpha-detector array was measured to be 2.69(1)% using a $^{148}$Gd calibration source mounted on the catcher foil frame. Alpha-array energy calibration is E = (0.0049 MeV/Ch)(Ch #) + 0.019 MeV.

The beta-array timing signal thresholds were set using the compton edge of the 0.662 MeV gamma-ray emitted from the decay of $^{137}$Cs. The pulse height of the 0.479 MeV compton edge was measured for each detector and the CFD thresholds were set for a pulse height that linearly scaled to a typical energy of 80 keV. A standard calibration source of $^{60}$Co was used to ensure that the proper delay times were set on each signal from the beta-detector array photomultiplier tubes to allow measurement of beta-particle and gamma-ray coincidence. The coincidence system for beta-particles and alpha-particles was checked using a standard $^{227}$Ac calibration source. This source emits alpha-particles and beta-particles in coincidence allowing tests of the TDC's and to properly select the timing gate to use for coincidence counting. Prior to data collection the complete timing system was tested with both $^{227}$Ac and $^{60}$Co calibration sources using data collection parameters to ensure all electronic components were properly set.

Coincidence spectra were in the typical decreasing time manner since a beta-particle is emitted prior to the alpha-particle starting an event. Lower alpha-particle energy starts an event later in time than a more energetic alpha-particle causing a shorter time difference between the alpha-particle and beta-particle. The gates for timing of alpha-beta coincidence was taken to be from a channel just above the $^{227}$Ac timing signal down 88 channels for each alpha-detector and beta-detector combination to ensure a gate width of 20 nanoseconds. This timing gate ensures detection of the beta-delayed alpha–decay of $^{20}$F since this coincidence should be about 10 nanoseconds less in time than the beta-delayed alpha–decay of $^{227}$Ac and it removes beta-gamma events since they occur at channels higher than the chosen gate. See figure 16 for the $^{227}$Ac alpha-particle energy spectrum in coincidence

with beta-particles using timing gates set for data analysis. This spectrum demonstrates that the timing gates were chosen correctly.

The gamma-decay of the $2^+$ state in $^{20}$Ne at 1.63 MeV in coincidence with the beta-particle emitted in the allowed beta-decay of $^{20}$F is shown in figure 17. This decay was used to normalize our first-forbidden rank-one beta-decay branching ratio measurements. We observed 88,887(1600) net counts for the 1.63 MeV peak of $^{20}$Ne after background subtraction. Background was measured by counting with an empty catcher foil frames under the same coincidence parameters used for data collection and normalized to the total beam during data collection. A normalization factor of 8.14(2) for this background was determined using Rutherford scattering of $^{19}$F off a 30 $\mu g/cm^2$ gold on 30 $\mu g/cm^2$ carbon foil as previously described. This allowed us to take into account $^{20}$F being deposited anywhere inside the vacuum chamber. Figure 18 shows the unnormalized gamma-ray background spectrum measured with the carbon catcher foils removed from the rotating arm. This method of background measurement was very effective in ensuring that we did not over subtract background. Only charged-particle and gamma-ray backgrounds capable of fulfilling coincidence requirements were subtracted from the coincidence spectrums.

Energy calibration and absolute efficiency of the HPGe detector was determined using standard $^{60}$Co, $^{137}$Cs, and $^{152}$Eu calibration sources. See figure 19 for $^{152}$Eu energy calibration spectra. These sources were placed on the catcher foil frames in place of the carbon catcher foils. Absolute efficiency measurement was performed using a least square fit of the data to a standard efficiency relationship, see equation 9 [SI76].

$$\varepsilon = (2.6 \times 10^{-4}) E_{(MeV)}^{-0.40} \qquad (9)$$

The calculated absolute HPGe detector efficiency was 2.1(3) x $10^{-4}$ for the 1.63 MeV gamma-ray emitted in the decay of the lowest $2^+$ state in $^{20}$Ne. The $^{152}$Eu and $^{60}$Co peaks were

corrected for sum loss fractions and sum gain fractions [GE77]. HPGe detector energy calibration is E = (0.002 MeV/Ch)(Ch #) - 0.015 MeV.

## Branching Ratio Measurements

We attempted to measure three $^{20}$F first-forbidden beta-decay branching ratios, one rank-zero decay and two rank-one decays. All three measurements were normalized to the allowed beta-decay of $^{20}$F to the $2^+$ state at 1.63 MeV in $^{20}$Ne that has a branching ration of 0.9999 [AJ83]. This $2^+$ state in $^{20}$Ne gamma-decays to the $0^+$ ground state in $^{20}$Ne with an energy of 1.63 MeV 100% of the time making it very useful for normalization [AJ83]. A total of 88887(1600) net counts were observed in the HPGe detector with an efficiency of 2.1(3) x $10^{-4}$ at 1.63 MeV.

The first-forbidden rank-zero beta-decay of $^{20}$F decays to the $2^-$ state at 4.97 MeV in $^{20}$Ne [AJ83]. This $2^-$ state in $^{20}$Ne subsequently gamma-decays to the $2^+$ state at 1.63 MeV in $^{20}$Ne with a branching ratio of 0.994 emitting a gamma-ray with an energy of 3.33 MeV [AJ78, AL81a]. A total of 8(3) net counts were observed in the HPGe detector with an efficiency of 1.6(3) x $10^{-4}$ at 3.33 Mev. The first-forbidden rank-zero beta-decay of $^{20}$F measured branching ratio is 1.2(6) x $10^{-4}$ and its log(*ft*) is 7.1(2). This confirms the branching ratio of 9.0(4) x $10^{-5}$ and log(*ft*) of 7.16(2) measured by Alburger and Warburton [AL81a].

The first-forbidden rank-one beta-decays of $^{20}$F were not observed in this experiment. The events observed in the regions of interest are consistent with background; therefore, only upperlimits for the branching ratios are calculated. A total of 7 counts are observed in the region of interest (0.64 MeV to 0.79 MeV) for the alpha-particle decay of the $3^-$ state at 5.62 MeV and 3 counts (0.77 MeV to 0.93 MeV) for the $1^-$ state at 5.79 MeV in $^{20}$Ne, both consistent with background. The branching ratios for alpha-decay are 0.927 and 0.999 for the $3^-$ and $1^-$ states, respectively. The calculated first-forbidden rank-one beta-decay branching ratio upperlimits at 2$\sigma$ are 1.5 x $10^{-6}$ and 7 x $10^{-7}$ for the $3^-$ state at 5.62 MeV and $1^-$ state at

5.79 MeV of $^{20}$Ne, respectively.

The upperlimits for the branching ratios gives estimates for the partial half-life lower limits to be 7.3 x $10^6$ seconds and 1.6 x $10^7$ seconds for the $3^-$ and $1^-$ states of $^{20}$Ne, respectively. Calculated $f$ values of 24.6(2.5) for the $3^-$ state and 14.6(1.5) for the $1^-$ state were obtained using the method outlined by E. Feenberg and G. Trigg [FE50]. The corresponding comparative half-lives or log($ft$) values are 8.2 and 8.3 for the $3^-$ and $1^-$ states of $^{20}$Ne, respectively.

The obtained branching ration upperlimits improve previous upperlimits by factors of 320 and 1428 for the first-forbidden rank-one beta-decays to the $3^-$ and $1^-$ states, respectively, of $^{20}$Ne. These upperlimits are considerably lower than predicted values for phase space corrections to the first-forbidden rank-zero branching ratio to the $2^-$ state at 4.97 MeV of $^{20}$Ne. They are consistent with the predicted values of 1.4 x $10^{-6}$ and 7 x $10^{-7}$ using phase space correction with E. K. Warburton's proposed correction to rank-zero matrix elements for the decay to the $3^-$ and $1^-$ states, respectively, of $^{20}$Ne.

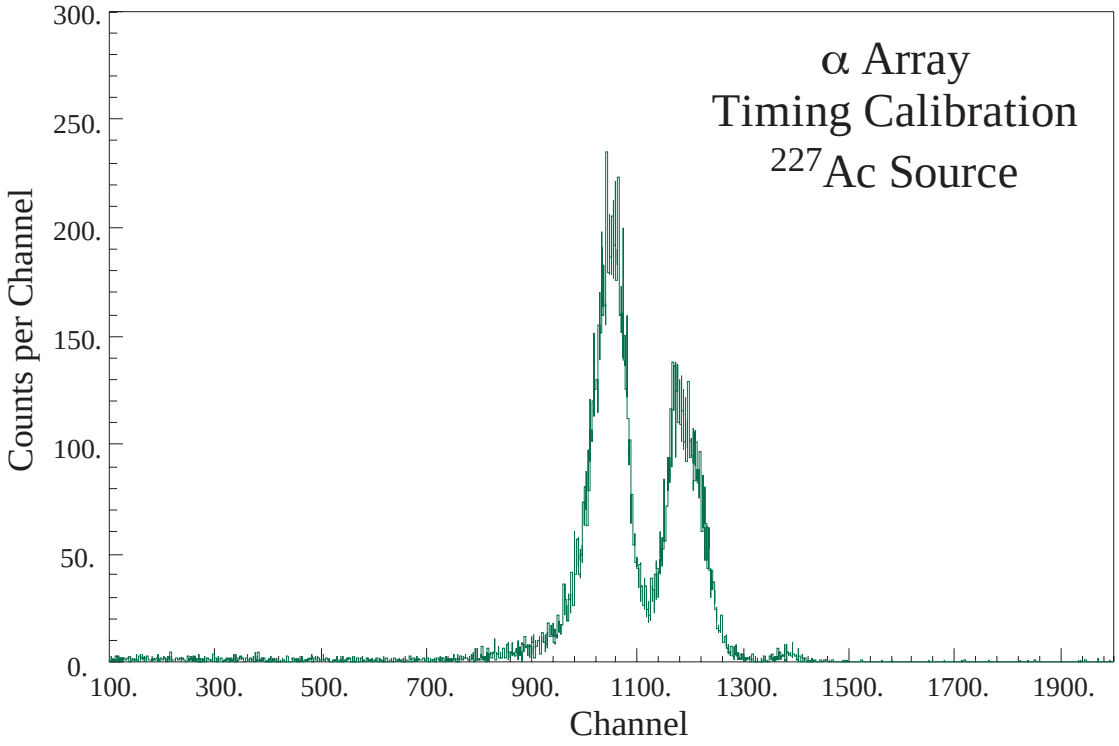


Figure 16 : Alpha-particle energy spectrum exhibiting beta-delayed alpha-decay of $^{227}$Ac calibration source using timing coincidence gates for data collection.

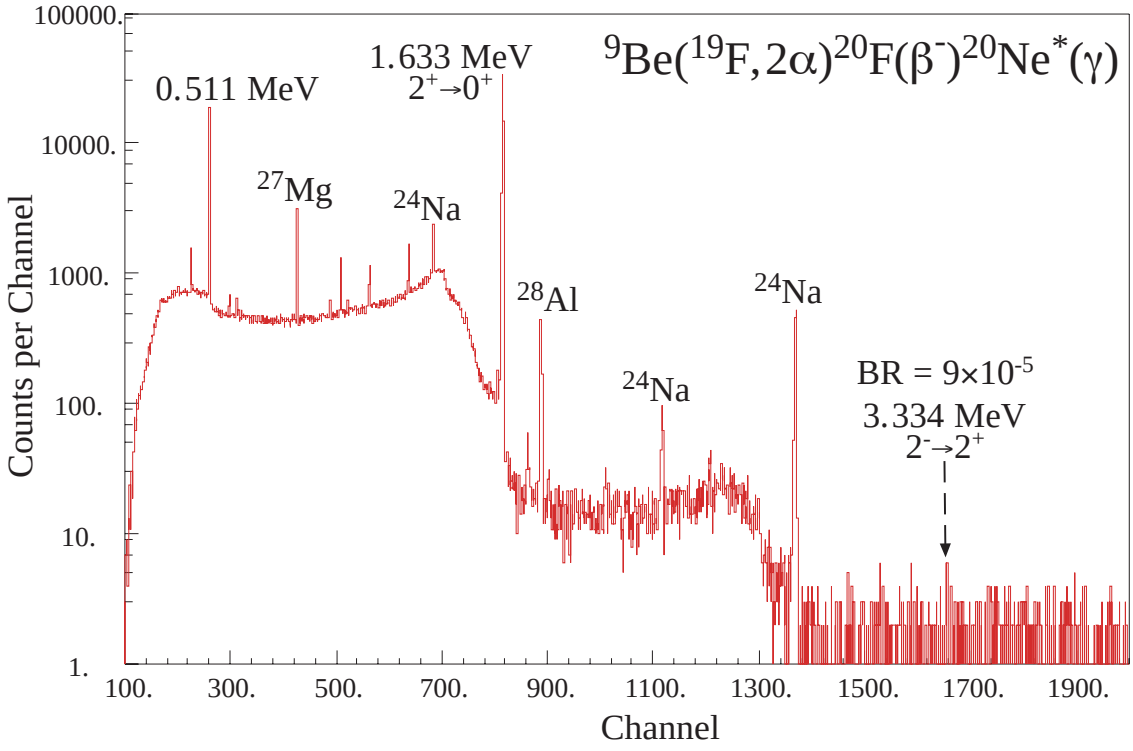


Figure 17 : Gamma-decay of $^{20}$Ne in coincidence with allowed beta-decay of $^{20}$F.

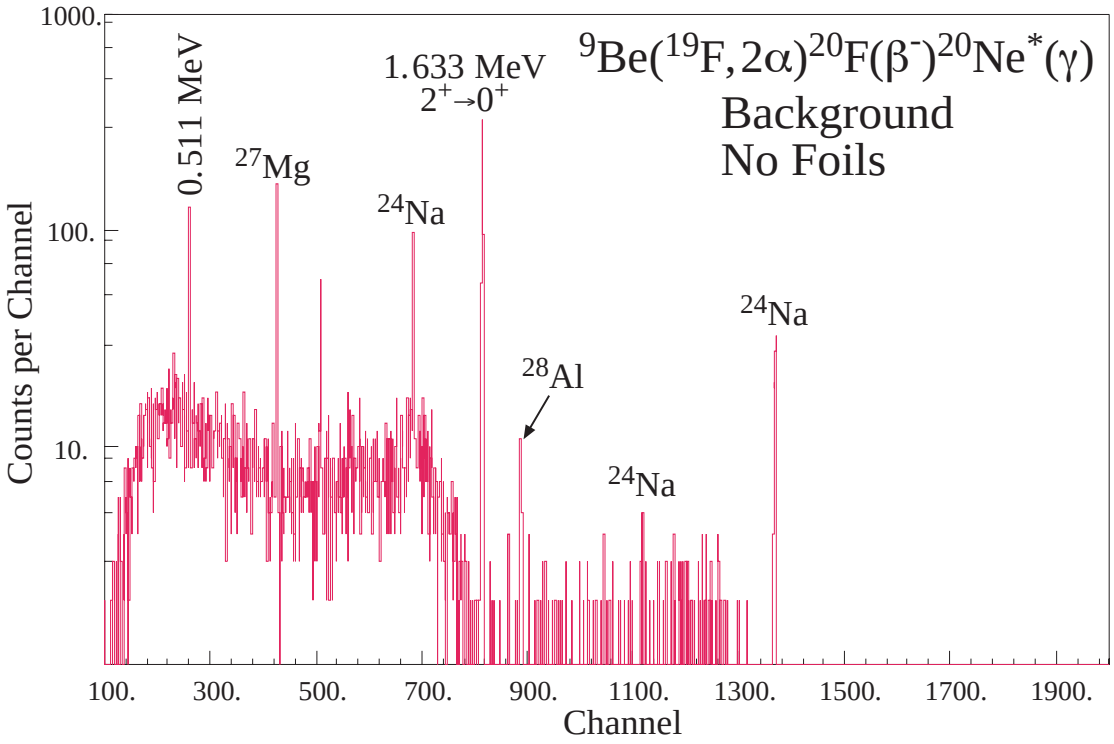


Figure 18 : Unnormalized Background spectrum for gamma-decay of $^{20}$Ne in coincidence with allowed beta-decay of $^{20}$F.

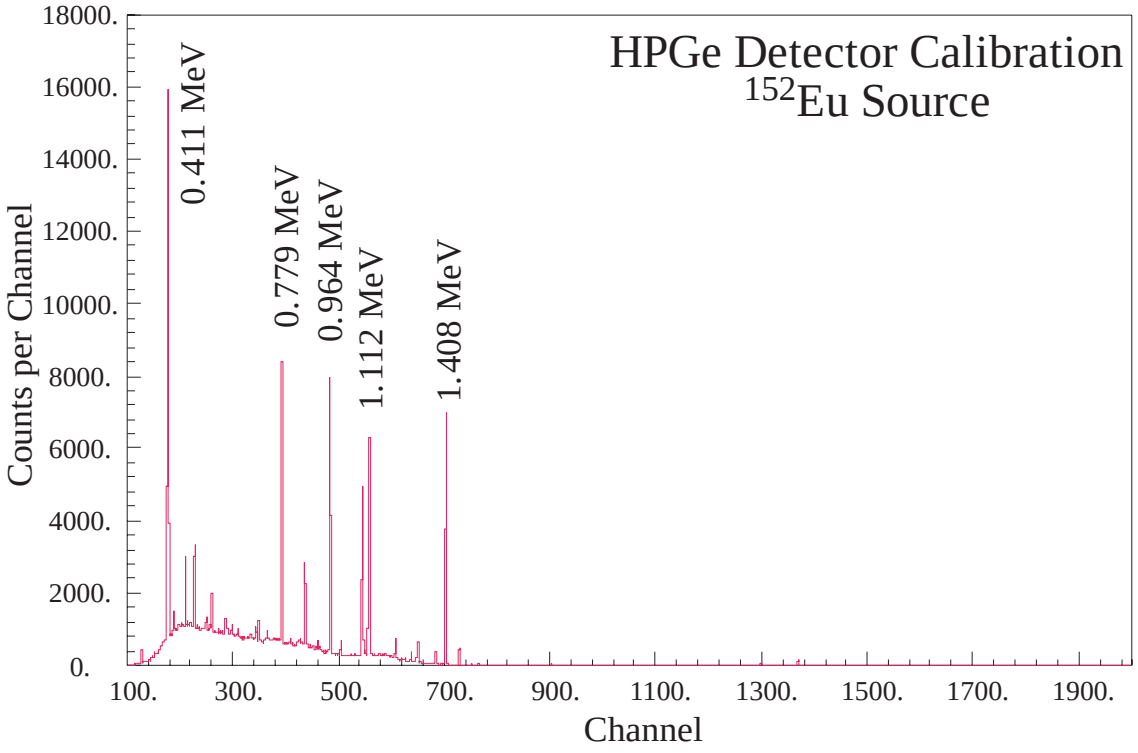


Figure 19 : HPGe detector gamma-ray energy calibration spectrum from $^{152}$Eu.

# CONCLUSION

Previously published upper limits for the first-forbidden rank-one beta-decay branching ratios of $^{20}$F were [AJ78]:

$< 4.8 \times 10^{-4}$ to the $^{20}$Ne $3^-$ state at 5.62 MeV.

$< 1 \times 10^{-3}$ to the $^{20}$Ne $1^-$ state at 5.79 MeV.

We determined the first-forbidden rank-one beta-decay branching ratio of $^{20}$F upper limits to be

$< 1.5 \times 10^{-6}$ to the $^{20}$Ne $3^-$ state at 5.62 MeV

and

$< 7 \times 10^{-7}$ to the $^{20}$Ne $1^-$ state at 5.79 MeV

at $2\sigma$. The obtained upper limits represent an improvement by a factor of 320, 1428 for the branching ratios to the $3^-$, $1^-$ states in $^{20}$Ne. These branching ratios are also considerably lower than the prediction based on phase space corrections the known branching ratio for the first-forbidden rank-zero beta-decay to the $2^-$ state at 4.97 MeV of $^{20}$Ne and are at the predicted values using E. K. Warburton's proposed corrections to the matrix elements.

Our branching ratio upperlimits give log(*ft*) values of 8.2 and 8.3 for the $3^-$ and $1^-$, respectively, and are within the expected range for first-forbidden beta-decay. The measured branching ratio of 1.2(6) x $10^{-4}$ for the first-forbidden rank-zero beta-decay of $^{20}$F to the $2^-$ state in $^{20}$Ne at 4.97 MeV results in a log(*ft*) of 7.1(2). This confirms the branching ratio measurement of 9.0(4) x $10^{-5}$ and log(*ft*) of 7.16(2) by Alburger and Warburton [AL81a].

The largest uncertainty in our measurement is due to the statistical uncertainty of

the total alpha-particle counts. As seen in the alpha-particle background spectrum, we obtained sufficiently low background and sensitivity to measure these first-forbidden rank-one beta-decay branching ratios.

# REFERENCES


[AD85] E. G. Adelberger and W. C. Haxton; *Ann. Rev. Nucl. Part. Sci.* **35** (1985) 501.

[AD91] E. G. Adelberger, A. Garcna, P. V. Magnus, and D. P. Wells; *Phys. Rev. Lett.* **67** (1991) 3658.

[AD93] E. G. Adelberger; *Phys. Rev. Lett.* **70** (1993) 2856.

[AJ78] F. Ajzenberg-Selove; *Nucl. Phys.* **A300** (1978) 184.

[AJ83] F. Ajzenberg-Selove; *Nucl. Phys.* **A392** (1983) 1.

[AJ87] F. Ajzenberg-Selove; *Nucl. Phys.* **A475** (1987) 1.

[AL81] D. E. Alburger, C. J. Lister, J. W. Olness, and D. J. Millener; *Phys. Rev. C* **23** (1981) 2217.

[AL81a] D. E. Alburger and E. K. Warburton; *Phys. Rev. C* **24** (1981) 296.

[BE96] Henri Becquerel; *Comptes rendus de l'Acdemie des Sciences* **122** (1896) 501, Translated and reprinted in Benchmark Papers in Physical Chemistry and Chemical Physics/5, Hutchinson Ross Publishing Co., Stroudsburg, Pennsylvania, 1982, ed. G. T. Seaborg and W. Loveland.

[BL64] R. J. Blin-Stoyle; Fundamentals of b- Decay Theory Selected Topics in Nuclear Spectroscopy, Proceedings of the NUFFIC International Summer Course in Science at Nijenrode Castle, The Netherlands, July 30 - August 17, 1963, North-Holland Publishing Company, Amsterdam, 1964, complied by B. J. Verhaar 199.

[BL79] John M. Blatt and Victor F. Weisskopf; Theoretical Nuclear Physics, Dover Publications, Inc., New York, 1979 by Springer-Verlag New York, Inc.

[BO58] F. Boehm, V. Soergel, and B. Stech; *Phys. Rev. Lett.* **1** (1958) 77.

[BO84] A. I. Boothroyd, J. Markey, and P. Vogel; *Phys. Rev. C* **29** (1984) 603.

[BR78] E. Browne, J. M. Dairike, R. E. Doebler, A. A. Shihab-Eldin, L. J. Jardine, J. K. Tuli, A. B. Buyrn; Table of Isotopes, 7th ed., John Wiley & Sons, New York, 1978.

[CA90] A. S. Carnoy, J. Deutsch, T. A. Girard, and R. Prieels; *Phys. Rev. Lett.* **65** (1990) 3249.

[Ch32] J. Chadwick; *Nature* **129** (1932) 312, Reprinted in Benchmark Papers in Physical Chemistry and Chemical Physics/5, Hutchinson Ross Publishing Co., Stroudsburg, Pennsylvania, 1982, ed. G. T. Seaborg and W. Loveland.

[DE64] J. Deutsch; Analysis of Some First Forbidden Beta Transitions and the Conserved Vector Current Theory of Weak Interaction Selected Topics in Nuclear Spectroscopy, Proceedings of the NUFFIC International Summer Course in Science at Nijenrode Castle, The Netherlands, July 30 - August 17, 1963, North-Holland Publishing Company, Amsterdam, 1964, complied by B. J. Verhaar 323.

[DE80] B. Desplanques, J. F. Donoghue, and B. R. Holstein; *Ann. Phys.* **124** (1980) 449.

[DE92] D. S. Delion, A. Insolia, and R. J. Liotta; *Phys. Rev. C* **46** (1992) 1346.

[FE33] Enrico Fermi; *Ric. Sci.* **4** (1933) 491, Translated and reprinted in Benchmark Papers in Physical Chemistry and Chemical Physics/5, Hutchinson Ross Publishing Co., Stroudsburg, Pennsylvania, 1982, ed. G. T. Seaborg and W. Loveland.

[FE50] E. Feenberg and G. Trigg; *Rev. Mod. Phys.* **22** (1950) 399.

[FO72] H. T. Fortune, G. C. Morrison, R. C. Bearse, J. L. Yntema, and B. H. Weldenthal; *Phys. Rev. C* **6** (1972) 21.

[FO74] H. T. Fortune, R. R. Betts; *Phys. Rev. C* **10** (1974) 1292.

[FR96] R. H. France III; Ph.D. Thesis, Yale University, 1996.

[GE76] H. Genz, A. Richter, B. M. Schmitz and H. Behrens; *Nucl. Phys.* **A267** (1976) 13.

[GE77] R. J. Gehrke, R. G. Helmer, and R. C. Greenwood; *Nucl. Instr. Meth.* **147** (1977) 405.

[GO58] Goldhaber, Grodzins and Synyar; *Phys. Rev.* **109** (1958) 1015.

[GU78] P. A. M. Guichon, M. Giffon, and C. Samour; *Phys. Lett.* **74B** (1978) 15.

[HA69] Bernard G. Harvey; Introduction to Nuclear Physics and Chemistry, 2nd ed., Prentice Hall, Englewood Cliffs, New Jersey, 1969.

[HU52] D. T. Hurd; An Introduction to the Chemistry of the Hydrides, John Wiley & Sons, Inc., New York, 1952.

[JU92] M. Jung, F. Bosch, K. Beckert, H. Eickhoff, H. Folger, B. Franzke, A. Gruber, P. Kienle, O. Klepper, W. Koenig, C. Kozhuharov, R. Mann, R. Moshammer, F. Nolden, U. Schaaf, G. Soff, P. Spädtke, M. Steck, Th. Stöhlker, and K. Sümmerer; *Phys. Rev. Lett.* **69** (1992) 2164.

[KN89] G. F. Knoll; Radiation Detection and Measurement 2nd Ed., John Wiley & Sons, Inc., New York, 1989.

[KO55] E. Konopinski; The Theory of Forbidden Beta-Decay in Beta- and Gamma-Ray Spectroscopy, North-Holland Publishing Company, Amsterdam, 1955, ed. K. Siegbahn, Chapter X.

[KR84] J. Krumlinde; *Nucl. Phys.* **A413** (1984) 223.

[KU78] K. Kubodera, J. Delorme, and M. Rho; *Phys. Rev. Lett.* **40** (1978) 755.

[LA72] S. Laribi, H. Beaumervieille, N. Bendjaballah, D. Lalanne, J. F. Allard, and B. Faid; *Nucl. Phys.* **A191** (1972) 368.

[LE67] F. A. Lewis; The Palladium Hydrogen System, Academic Press, New York, 1967.

[MA58] I. Marklund and L. A. Page; *Nucl. Phys.* **9** (1958) 88.

[MI82] D. J. Millener, D. E. Alburger, E. K. Warburton, and D. H. Wilkinson; *Phys. Rev. C* **26** (1982) 1167.

[MO77] C. A. Mosley Jr. and H. T. Fortune; *Phys. Rev. C* **16** (1977) 1697.

[PA34] W. Pauli; *Structure et Proprietes des Noyaux Atomique* (1934) 324, Translated and reprinted in Benchmark Papers in Physical Chemistry and Chemical Physics/5, Hutchinson Ross Publishing Co., Stroudsburg, Pennsylvania, 1982, ed. G. T. Seaborg and W. Loveland.

[RE84] H. R. Reiss; *Phys. Rev. C* **29** (1984) 2290.

[RI90] A. Richter, A. Weiss, O. Haüsser, and B. A. Brown; *Phys. Rev. Lett.* **65** (1990) 2519.

[RO55] M. E. Rose; The Theory of Allowed Beta-Decay in Beta- and Gamma-Ray Spectroscopy, North-Holland Publishing Company, Amsterdam, 1955, ed. K. Siegbahn, Chapter IX.

[RO93] M. W. Rota and E. L. Wilds; *ORNL Rad. Shield. Info. Ctr. Lib.* (1993) MeV Computer Code.

[RU03] E. Rutherford and F. Soddy; *Phil. Mag.* **5** (1903) 576, Reprinted in Benchmark Papers in Physical Chemistry and Chemical Physics/5, Hutchinson Ross Publishing Co., Stroudsburg, Pennsylvania, 1982, ed. G. T. Seaborg and W. Loveland.

[SC66] Herwig F. Schopper; Weak Interactions and Nuclear Beta Decay, North-Holland Publishing Company, Amsterdam, 1966.

[SE72] Henry Semat and John R. Albright; Introduction to Atomic and Nuclear Physics, Holt, Rinehart and Winston, Inc., New York, 1972.

[SE73] Standard Mathematical Tables, The Chemical Rubber Co., Cleveland, 1973, Editor-in-Chief of Mathematics Samual M. Selby.

[SH67] B. L. Shaw; Inorganic Hydrides, Pergamon Press, Oxford, 1967.

[SI76] R. Singh; *Nucl. Instr. Meth.* **136** (1976) 543.

[SP61] F. H. Speding and A. H. Daane; The Rare Earths, John Wiley & Sons, Inc., New York, 1961.

[TO86] I. S. Towner; *Ann. Rev. Nucl. Part. Sci.* **36** (1986) 115.

[TO86a] I. S. Towner; *Comments Nucl. Part. Phys.* **15** (1986) 145.

[TO92] I. S. Towner; *Nucl. Phys.* **A542** (1992) 631.

[VA92] K. Varga, R. G. Lovas, and R. J. Liotta; *Phys. Rev. Lett.* **69** (1992) 37.

[WA81] E. K. Warburton and D. E. Alburger; *Phys. Rev. C* **23** (1981) 1234.

[WA82] E. K. Warburton, D. E. Alburger, and D. H. Wilkinson; *Phys. Rev. C* **26** (1982) 1186.

[WA84] E. K. Warburton, D. E. Alburger, and D. J. Millener; *Phys. Rev. C* **29** (1984) 2281.

[WA86] E. K. Warburton; *Phys. Rev. C* **33** (1986) 303.

[WA91] E. K. Warburton; *Phys. Rev. C* **44** (1991) 233.

[WA91a] E. K. Warburton; *Phys. Rev. C* **44** (1991) 261.

[WA91b] E. K. Warburton; *Phys. Rev. C* **44** (1991) 268.

[WA91c] E. K. Warburton; *Phys. Rev. Lett.* **66** (1991) 1823.

[WA92] E. K. Warburton and I. S. Towner; *Phys. Lett. B* **294** (1992) 1.

[WA94] E. K. Warburton, I. S. Towner, and B. A. Brown; *Phys. Rev. C* **49** (1994) 824.

[WI94] E. L. Wilds, R. H. France III, and M. Gai; *Bull. Amer. Phys. Soc.* **39** (1994) 1241.

[WO90] Samuel S. M. Wong; Introductory Nuclear Physics, Prentice Hall, Englewood Cliffs, New Jersey, 1990.

[WU55] C. S. Wu; Experiments on the Shape of b-Spectra The Interaction in b-Decay in Beta- and Gamma-Ray Spectroscopy, North-Holland Publishing Company, Amsterdam, 1955, ed. K. Siegbahn, Chapter XI.

[WU57] C. S. Wu, E. Ambler, R. W. Hayward, D. D. Hoppes, and R. Pl Hudson; *Phys. Rev.* **105** (1957) 1413.

[ZH92] Z. Zhao; Ph.D. Thesis, Yale University, 1992.

[ZH92a] Z. Zhao, R. H. France III, K. S. Lai, M. Gai, E. L. Wilds; *Bull. Amer. Phys. Soc.* **37** (1992) 1256.

[ZI91] J. F. Ziegler and J. P. Biersack; *Code TRIM 91*.